



Politecnico
di Torino



Master's Degree in Aerospace Engineering

Mission and System Design of a Formation-Flying Picosatellites Cluster: A Technology Demonstration Mission for Space Situational Awareness Improvement

Supervisors:

Prof. Fabrizio STESINA, Politecnico di Torino

Prof. Stefano SPERETTA, TU Delft

Co-Supervisors:

Prof. Nicole VIOLA, Politecnico di Torino

Res. Mehmet Şevket ULUDAĞ, TU Delft

Candidate:

Marianna CENTRELLA

Politecnico di Torino

A.Y. 2022/2023

Per Aspera ad Astra.

Acknowledgements

I would like to express my deepest gratitude to Prof. Stefano Speretta, who allowed me to write this thesis at TU Delft and patiently guided me through every stage of the project with his remarkable knowledge and professionalism.

I am very thankful to Prof. Fabrizio Stesina who, with regular meetings and valuable advice, has always supported my research work from Politecnico di Torino.

A special thank you to Res. Mehmet Şevket Uludağ who, with his great experience, helped and encouraged me every day. Thank you to Prof. Nicole Viola, for having been always available to me. I would like to thank all the people from the TU Delft - Faculty of Aerospace Engineering, Space Systems Engineering Department, headed by Prof. Eberhard Gill, for welcoming me in these months. Thank you to all the PhD candidates for every coffee break and precious advice shared.

My heartfelt thank you to my mother and my father, for the life values they instilled in me and for their unwavering support over the years. They have enabled me to live incredible experiences and achieve my goals, turning my dreams into reality. To both of you, I extend my gratitude. Thank you to my grandmother for her immeasurable love and to my grandfather for his curiosity, for every time he asked me how far Earth was from Mars. Thank you to my beloved siblings, my brother and my sister, pillars of my life. With each other, we have never felt alone, and we never will. Thank you to my whole family and my lifelong friends for always being by my side. A sincere thank you to my 'Turin Family', my dearest friends. To those who shared the university journey with me, encouraging me to never give up even in the most challenging times. Always wearing a smile, ready to actively listen, have fun, and travel together around Europe. Thank you to all my friends from my hometown, from AESA (Aerospace Engineering Students' Association), the CubeSat Team, SGAC, ESA Academy, and to my international friends I met in The Netherlands. You all have a special place in my heart.

Torino, October 25th, 2023

Marianna Centrella

Abstract

In recent years, nano- and pico-satellite missions have risen in popularity due to the availability of affordable launches and enhanced technology to enable smaller instruments and subsystems. As space traffic increases, especially in Low Earth Orbit (LEO), the trend toward miniaturization has raised concerns in the space community. These small objects may approach the threshold of current tracking capabilities, potentially becoming space debris if they cannot be successfully identified and tracked. To pioneer space research and technology, Delft University of Technology aims to develop a mission consisting of multiple picosatellites to demonstrate the capabilities and limits of in-space and ground-based tracking means.

Within this framework, the thesis focuses on the high-level mission analysis and system design of a formation-flying cluster of two PocketQubes, as part of this novel technology demonstration mission for Space Situational Awareness (SSA) improvement. Launched as a single spacecraft, once in orbit the PocketQubes will be detached in two identical and independent twin satellites.

The use of Systems Tool Kit (STK) software allowed to create several scenarios, including both space and ground segments, and to build different Mission Control Sequences (MCS) for each satellite. Through the interface between STK and MATLAB environment, the sequences were used to analyse the satellite in-flight separation in terms of direction and detachment angles, the satellite undocking velocities and the consequences of drag area variations, achievable for instance by exploiting deployable solar panels. Using differential drag control led to the investigation of what occurred during the first satellite conjunctions and also affected the mission lifetime, for which at least some months of in-orbit testing had to be ensured.

The simulations confirmed the mission feasibility and allowed to identify and collect high-level mission requirements. Their elicitation continued with a focus on the orbit average power, performing a power budget analysis to estimate the power available for payload functioning. Among the payloads, a Global Navigation Satellite

System (GNSS) receiver will be included in each satellite equipment, thus making the satellite independent in orbital determination, and providing a way to validate its position data with respect to other tracking systems. An extensive study on the GNSS receivers was conducted to define a possible candidate among space-capable Commercial Off-the-Shelf (COTS) receivers.

The mission and system requirements obtained will be used as input for detailed mission analysis, such as finding the optimum satellite control strategy in Close Proximity Operations (CPO), and for future iterations of payload design.

Contents

List of Figures	xi
List of Tables	xv
Acronyms / Abbreviations	xvii
1 Introduction	1
1.1 PocketQubes	1
1.1.1 The Rise of Nanosatellites	1
1.1.2 The PocketQube Standard	3
1.2 A Novel Picosatellites Mission	4
1.2.1 The Delfi Program	4
1.2.2 Mission Description and Goals	6
1.2.3 Project Timeline	9
1.2.4 Mission Architecture and Payloads	9
1.3 Research Framework and Goals	11
1.3.1 Satellite in-Flight Separation and Control via Differential-Drag	11
1.3.2 High-level Requirements Elicitation	12
1.3.3 Payload High-Level Design: the GNSS Receiver	12
1.3.4 Thesis Outline	13

2	The Basics of Orbital Mechanics	14
2.1	Reference Frames and Coordinate Systems	14
2.1.1	Earth-Centered Inertial Reference Frame	14
2.1.2	Earth-Centered Earth-Fixed Reference Frame	15
2.1.3	Radial In-Track Cross-Track Coordinate System	16
2.2	The Two-Body Problem	17
2.3	Orbital Elements	19
2.4	Perturbative Accelerations	20
2.4.1	Atmospheric Drag	21
2.4.2	Solar Radiation Pressure	22
2.4.3	Third-Body Effects	23
2.5	Orbital Maneuvers	23
2.5.1	Orbital Maneuvers from a Stable Relative Position and their Effects	23
3	Mission Analysis	26
3.1	Scenario Definition and Implementation in STK	26
3.1.1	Analysis Period	27
3.1.2	Space and Ground Segments	27
3.1.3	Satellite Control Sequences	29
3.2	Integration with MATLAB	37
3.3	DRAMA Tool Setup	39
4	Simulation Results and High-Level Requirements	41
4.1	Space Segment Analyses	41
4.1.1	Direction of Separation	42
4.1.2	Separation Velocity	44

4.1.3	Drag Area Control: Stopping Conditions based on Relative Distance	45
4.1.4	Drag Area Control: Stopping Conditions based on Relative Distance and Relative Velocity	48
4.1.5	Limiting Angle of Separation	52
4.2	Orbital Lifetime Variations	63
4.2.1	Simulation: Sequence 1	63
4.2.2	Simulation: Sequence 2	64
4.3	Accesses	65
4.3.1	Accesses between Satellites and Radio Ground Station . . .	65
4.3.2	Accesses between Satellites and Optical Ground Station . .	65
5	GNSS Receiver High-Level Design	66
5.1	The Basics of Global Navigation Satellite System	66
5.2	Power Analysis	68
5.2.1	Orbit Average Available Power	68
5.2.2	Power Budget	70
5.2.3	Possible GNSS Receivers for the TU Delft Mission	72
5.3	GNSS Signal Emulation	75
5.3.1	Software-Defined GPS Signal Simulator (GPS-SDR-SIM) .	75
5.3.2	GNSS Receiver Software	76
5.3.3	Hardware-In-The-Loop Simulation: Setup and Process . . .	77
5.3.4	Hardware-In-The-Loop Simulation: Accuracy of the GNSS Receiver	80
5.3.5	GNSS Receiver Power Consumption	89
6	Conclusions and Future Work	90
6.1	Conclusions	90

6.2	Future Work	93
	References	95
	Appendix A Technical Requirement Specification	100
A.1	Initial Mission and System Requirements	102
A.2	New Mission and System Requirements	102
A.3	Applicable and Reference Documents	102

List of Figures

1.1	CubeSat Dimensions (non-scale).	2
1.2	PocketQube Dimensions (non-scale).	3
1.3	PocketQube Reference Axes and Sliding Backplate.	4
1.4	TU Delft previous nanosatellites.	5
1.5	The potential collision between two satellites would decrease if the uncertainty of satellite positioning was reduced. Source: GAO analysis of Department of Defense, National Oceanic and Atmospheric Administration, and The Aerospace Corporation images and information.	7
2.1	ECI and ECEF Reference Frames; RIC Coordinate System.	17
2.2	The Two-Body Problem.	18
2.3	Classical Orbital Elements.	20
2.4	Burns and Satellite Relative Motion.	24
3.1	FirstQube (green RIC axes) and SecondQube (red RIC axes) at the beginning of a scenario, shortly after their separation.	28
3.2	Scenario Objects as defined in STK.	29
3.3	This graphical representation (not to scale) is independent of time and actual orbits and is only intended to show the relative position of satellites as a result of changes to the drag area made during the implementation of a MCS with Sequence 1.	34

3.4	This graphical representation (not to scale) is independent of time and actual orbits and is only intended to show the relative position of satellites as a result of changes to the drag area made during the implementation of a MCS with Sequence 2.	37
3.5	STK and MATLAB interface in the context of this work.	38
3.6	Orbital elements and spacecraft parameters in DRAMA	39
4.1	RIC Reference Frame centered on FirstQube.	42
4.2	Relative distance as a function of the direction of separation. Analysis periods: 6 hours, 1 month.	43
4.3	Relative distance as a function of the increasing Separation Velocity. Analysis period: 1 week.	44
4.4	Relative distance as a function of a fixed Separation Velocity and increasing Drag Area. Analysis period: 1 month.	45
4.5	Relative velocity as a function of a fixed Separation Velocity and increasing Drag Area. Analysis period: 1 month.	46
4.6	Relative distance as a function of a fixed Separation Velocity and increasing Drag Area. Analysis period: 2 months.	47
4.7	Relative velocity as a function of a fixed Separation Velocity and increasing Drag Area. Analysis period: 2 months.	47
4.8	Relative distance calculated with the two control strategies. Increase and decrease in Drag Area once per satellite. Period of analysis: 1 month.	49
4.9	Relative velocity calculated with the two control strategies. Increase and decrease in Drag Area once per satellite. Period of analysis: 1 month.	49
4.10	Average relative velocity calculated with the two control strategies. Increase and decrease in Drag Area once per satellite. Period of analysis: 1 month.	50
4.11	Relative distance calculated with Sequence 2. Increase and decrease in Drag Area twice per satellite. Period of analysis: 2 months.	51

4.12	Zoom in on points of minimum relative distance between satellites. . .	52
4.13	Radial / In-Track / Cross-Track (XYZ) reference system centered on FirstQube, in STK. Azimuth (Az) and Elevation (El) angles are shown.	54
4.14	Azimuth and Elevation angles shown in different Reference Frames.	54
4.15	Relative Distance over time, calculated for 14 Azimuth angles. The Elevation angle is equal to zero. Period of analysis: 4 months. . . .	56
4.16	Zoom on the first satellite orbit of Figure 4.15 to highlight the points of minimum distance.	56
4.17	Minimum distance as a function of the Azimuth Angle.	57
4.18	Relative Distance over time, calculated for 14 Elevation angles, while the Azimuth angle is equal to zero. Period of analysis: 4 months.	58
4.19	Zoom in on the first satellite orbit to highlight the points of minimum distance. Period of analysis: 4 months.	58
4.20	Minimum distance as a function of the Elevation Angle.	59
4.21	Limiting Angles from Simulation 3 and 4.	61
4.22	The set of points that defines the region of space for which satellite separation leads to a relative distance greater than 1 km at the first close approach.	62
4.23	Altitude vs. Time for Simulation 1	63
4.24	Altitude vs. Time for Simulation 2	64
5.1	AzurSpace Solar Cell, from its Datasheet.	69
5.2	Solar Cells of the 3U CubeSat model in STK.	70
5.3	SkyTraq PX1122C GNSS Receiver.	74
5.4	SkyTraq S1216F8-GI3 GNSS Receiver.	74
5.5	Screenshot of the GNSS Viewer Software interface after the receiver has acquired the 3D-Fix during a simulation.	76
5.6	URSP Radio (a) and Attenuator (b).	78

5.7	SkyTraq PX1122C GNSS Receiver installed on its board (a) and DC Block (b).	78
5.8	The 3D graphs show the nearly perfect overlap between the input position (in blue) and the simulated position (in red). The axis limits are specified.	84
5.9	Position Errors related to "Initial State" Trajectory Arc.	85
5.10	Position Errors related to "Increase" Trajectory Arc.	86
5.11	Position Errors related to "Conjunction" Trajectory Arc.	86
5.12	Position Errors related to "Stop Scenario" Trajectory Arc.	87

List of Tables

1.1	Small satellites mass categories.	2
1.2	PocketQube External and Sliding Backplate Dimensions.	4
1.3	Project Phases.	6
1.4	Mission Payloads.	10
3.1	Orbital Elements of the spacecrafts.	30
3.2	Spacecraft Parameters set in STK.	30
3.3	Mission Control Sequences. All the Stopping Conditions (SC) after the satellites separation are based on the relative distance.	33
3.4	Mission Control Sequences. The Stopping Conditions (SC) after the satellites separation are based on both the relative distance and the relative velocity.	36
4.1	Initial MCSs for separation direction analysis.	42
4.2	Azimuth and Elevation angles for Simulation 1.	55
4.3	Azimuth and Elevation angles for Simulation 2.	57
4.4	Azimuth and Elevation angles for Simulation 3.	59
4.5	Azimuth and Elevation angles for Simulation 4.	60
4.6	Azimuth and Elevation Limit angles.	60
5.1	AzurSpace Solar Cell features and Number of Cells in a 3P PocketQube.	69

5.2	STK Solar Cell features and Number of Cells in the 3U CubeSat model.	69
5.3	TwinSat Mission Power Budget for Nominal Mode.	71
5.4	Contingency Values.	71
5.5	Space-capable and future candidate space-capable GNSS Receivers suitable for the TwinSat Mission. *N/A stands for Not Available. . .	73
5.6	Latitude, Longitude and Altitude coordinates of the radio ground station given as input for the simulation with SkyTraq PX1122C receiver.	80
5.7	User Motion File for "Initial State" trajectory arc.	82
5.8	Log File for "Initial State" trajectory arc.	83
5.9	Updated TwinSat Mission Power Budget for Nominal Mode, taking into account GNSS receiver payload power consumption.	89
A.1	Configuration Items.	101
A.2	Applicable and Reference Documents.	102
A.3	Initial Mission and Systems Requirements.	103
A.4	New Mission and Systems Requirements.	104

Acronyms / Abbreviations

AD Applicable Document

ADCS Attitude Determination and Control System

AGI Analytical Graphics Inc.

BEE Best Engineering Estimate

BIN Binary

CDH Command and Data Handling System

CEP Circular Error Probability

CI Configuration Item

CoCom Coordinating Committee for Multilateral Export Controls

COEs Classical Orbital Elements

COLLADA COLLaborative Design Activity

COM Communication Port

COM Component Object Model

COMM Communication System

COTS Commercial Off-The-Shelf

CSV Comma-Separated Values

DA Drag Area

DOD	Department Of Defense
DRAMA	Debris Risk Assessment and Mitigation Analysis
ECEF	Earth-Centered Earth-Fixed
ECI	Earth-Centered Inertial
ECSS	European Cooperation for Space Standardization
EGM	Earth Gravitational Model
EPS	Electrical Power System
ESA	European Space Agency
ESOC	European Space Operations Centre
ESTEC	European Space Research and Technology Centre
EU	European Union
FC	Future Candidate
FCA	First Close Approach
FM	Flight Model
FOM	Figure of Merit
FOV	Field Of View
GAGAN	GPS-Aided Geo-Augmented Navigation
GAO	Government Accountability Office
GNSS	Global Navigation Satellite System
GPS	Global Positioning System
GS	Ground Station
HPOP	High-Precision Orbit Propagator
HPOP	Horizontal Dilution of Precision

ID	Identifier
LED	Light-Emitting Diode
LEO	Low Earth Orbit
LLA	Latitude Longitude Altitude
LNA	Low Noise Amplifier
MCS	Mission Control Sequence
MRFOD	Morehead Rome Femtosatellites Orbital Deployer
MSU	Morehead State University
N/A	Not Available
NASA	National Aeronautics and Space Administration
NavIC	Navigation with Indian Constellation
NAVSOL	NAVigation SOLution
NMEA	National Marine Electronics Association
OSCAR	Orbital Spacecraft Active Removal
PNT	Positioning Navigation Timing
POD	Precise Orbit Determination
PQ	PocketQube
QZSS	Quasi-Zenith Satellite System
RAAN	Right Ascension of the Ascending Node
RD	Reference Document
RF	Radio Frequency
RIC	Radial In-Track Cross-Track
RINEX	Receiver Independent Exchange Format

RMSE	Root Mean Square Error
ROD	Review Of Design
RP	Radiation Pressure
SC	Stopping Conditions
SDR	Software-Defined Radio
SNR	Signal-to-Noise Ratio
SPC	SPace Capable
SSA	Space Situational Awareness
STK	Systems Tool Kit
STR	Structural System
TCS	Thermal Control System
TLE	Two Line Element
TTFF	Time To First Fix
TU Delft	Technische Universiteit Delft
UCS	Union of Concerned Scientists
UMF	User Motion File
US	United States
USB	Universal Serial Bus
USRP	Universal Software Radio Peripheral
UTC	Coordinated Universal Time
UTCG	Coordinated Universal Time Gregorian
WGS	World Geodetic System

Chapter 1

Introduction

This thesis focuses on the high-level mission analysis and system design of a new space mission currently under development at Delft University of Technology. The legacy of previously launched satellites will pioneer the design of a mission composed of multiple picosatellites, including at least two PocketQubes.

In this chapter, the historical background, the context and the objectives of the research will be introduced. The last paragraph will present the dissertation outline, briefly explaining the content of each following chapter.

1.1 PocketQubes

1.1.1 The Rise of Nanosatellites

Nowadays small satellites play a key role in space missions, ranging from Earth observation and technology demonstration to scientific research and planetary science purposes. As their level of complexity is generally lower than larger satellites, their development time is shorter, and thus their production rate increases [1]. They also usually carry fewer payloads, which contributes to a reduction in cost, further amplified by the extensive use of Commercial Off-The-Shelf¹ components. Small satellites also have drawbacks, such as typical limited lifetime, due to small subsystem sizes that tend to limit available power or the communication and propulsion

¹COTS are defined as "commercial electronic component readily available off-the-shelf, and not manufactured, inspected or tested in accordance with military or space standards". [2]

subsystem performance, and lower reliability, caused by less subsystem redundancy. However, they are widely used for various applications, particularly in educational and technology demonstration missions. In the latest years, nano- and pico-satellite missions have increased in popularity due to the availability of affordable launch opportunities and advanced technology that allowed to scale down instrument and subsystem dimensions.

As stated in State-of-the-Art of Small Spacecraft Technology [3], small satellites are generally grouped according to different categories:

Table 1.1 Small satellites mass categories.

Satellites Class Definition	Mass [kg]
Minisatellites	100 - 180
Nanosatellites	10 - 100
Picosatellites	0.1 - 1
Femtosatellites	0.01 - 0.1

The Microsatellites and Nanosatellites categories include CubeSats, a class of miniaturized satellites with standardized size, shape and mechanical interfaces. The first CubeSat platform dates back to early 2000s and was made of a single unit of 10 cm \times 10 cm \times 10 cm, which represents a form factor of 1U (see Figure 1.1, from [4]). Nowadays, even though 1U CubeSat are still developed, it is quite widespread to design bigger CubeSats by combining more units. For example, other typical standard form factors are 3U, 6U, 12U or even 27U.

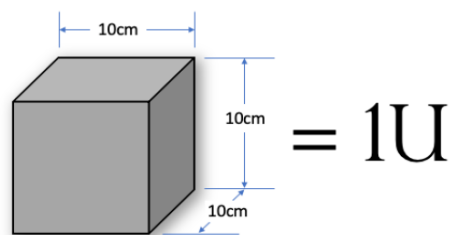


Fig. 1.1 CubeSat Dimensions (non-scale).

However, the focal point of this thesis will be hinged on another class of satellite, the Picosatellites, and specifically on PocketQubes (PQs), that fall in the latter category.

The PocketQube platform has a size of 50 mm x 50 mm x 50 mm, which represents a PocketQube unit, or 1P, equal to one-eighth the volume of a CubeSat [3] (see Figure 1.2, from [5]). Similar to CubeSats, also PocketQubes can be stacked together to create larger form factors, as 3P or 6P.

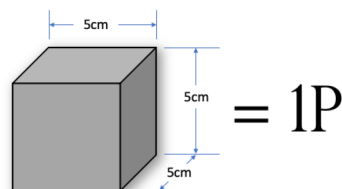


Fig. 1.2 PocketQube Dimensions (non-scale).

The trend toward miniaturization continued with the creation of this new standard that aimed to increase production rate and reduce launch costs. Indeed, by decreasing the satellite's volume by one-eighth compared to a CubeSat, its launch cost would be equally reduced. There was a need for a satellite "practical and affordable", that could fit in your pocket, and would spark the interest of the space community, ranging from universities to kick-starters companies. Professor Twiggs first proposed the PocketQube concept in 2009 [6], in collaboration with Morehead State University (MSU) and Kentucky Space. Back in 2013, the first four PQs were launched on a Dnepr rocket. They were carried on UniSat-5 microsatellite and deployed through the Morehead Rome Femtosatellites Orbital Deployer (MRFOD). In recent years, launches with Picosatellites have remarkably increased, and by June 2023, 61 PQs have successfully been launched [5] [7]. Most of them are still operational in orbit, while around 40 new PQs are currently under development.

1.1.2 The PocketQube Standard

To raise its popularity in the space community, a PocketQube Standard [8] was created by a joint effort of Alba Orbital, Delft University of Technology and GAUSS Srl. Its primary goal is to provide specifications for the design and development of PQs, defining common standards and interfaces for the PocketQube platform. The document comprises general and mechanical requirements and specifies the PQ external dimensions. The latter are influenced by a sliding backplate which the PQs uses for ejection, in contrast to the CubeSats, usually deployed along its long-side

edges. These dimensions are defined in the Table 1.2 for a 3P PocketQube, while the sliding backplate is clearly observable in the next Figure (from [8], together with axis specification.)

Table 1.2 PocketQube External and Sliding Backplate Dimensions.

Number of Units (P)	External Dimensions without Backplate [mm]	Sliding Backplate Dimensions [mm]
3P	50x50x178	58x192x1.6

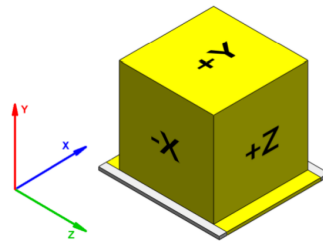


Fig. 1.3 PocketQube Reference Axes and Sliding Backplate.

1.2 A Novel Picosatellites Mission

1.2.1 The Delfi Program

The Delfi Space Program is a design and development line of nanosatellites at TU Delft [9]. Started in 2004, its first goal is to educate students with technical competencies and team skills, providing them with an overview of real space missions. It also aims to test and qualify disruptive space technologies and to improve the small satellites bus platforms targeted for novel future applications. The three technology missions that Delfi Program includes so far will be introduced, delving more deeply into the last one, as it is a crucial reference for this thesis.

- **Delfi-C³**. Launched in 2008, it is the first TU Delft and Dutch nanosatellite. After 15 years, this 3U CubeSat is still operational.
- **Delfi-n3Xt**. Launched in 2013, it also is a triple-unit CubeSat. The satellite was operational until 2014, having achieved its mission objectives.

- **Delfi-PQ.** Launched in early 2022, it is a 3P PocketQube with a mass of approximately 0.6 kg that paved the way for a strong trend towards space technology miniaturization. The mission aimed to demonstrate a reliable core bus platform (fitting in 1P volume), to test the external structure for this new form factor and at least one advanced subsystem or a scientific payload [10]. Successfully achieved its goals, the mission is still operational.

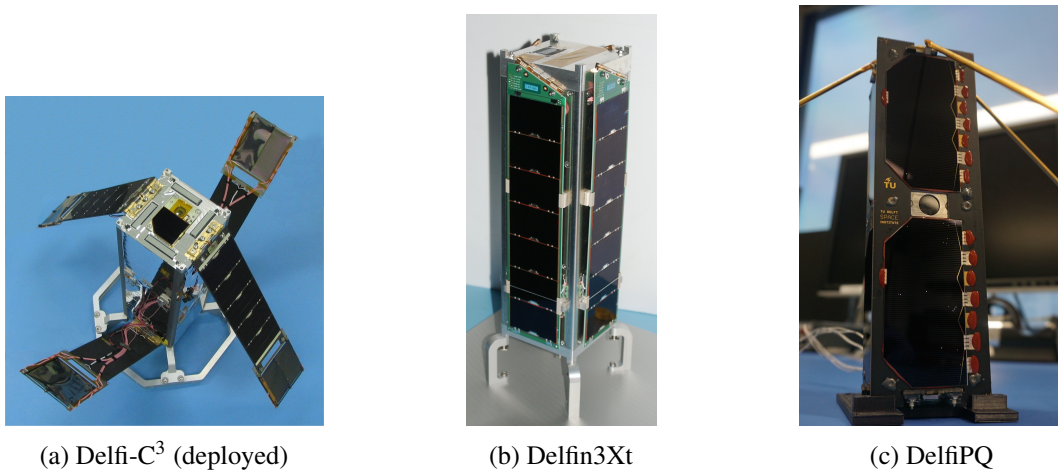


Fig. 1.4 TU Delft previous nanosatellites.

The knowledge and expertise gained from the past, and especially from Delfi-PQ, will be leveraged to continue developing new missions. The first major short-term goal could be summarized as "going small," meaning the trend toward miniaturization will rise with the development of pico- and femto-satellites. Missions with multiple satellites will be launched, for example to test and qualify autonomous formation-flying, to enable TU Delft to pioneer cutting-edge space research and technology, not only in academia. Furthermore, beyond technological demonstration and platform innovation, the educational purpose have always played a primary role in the Delfi Team missions. To allow students to have the opportunity to constantly get hands-on experience throughout the end-to-end development of a satellite, ideally a small satellite platform should always be in-development in the Clean Room, thus ensuring a launch opportunity every two or three years. Within this vision, a novel mission is currently being conceptualized. This thesis project was carried out within the scope of this mission, which as of today is in its 0/A phase [11].

Table 1.3 Project Phases.

Space Project Lifecycle	
Phase 0	Mission analysis / needs identification
Phase A	Feasibility
Phase B	Preliminary Definition
Phase C	Detailed Definition
Phase D	Qualification and Production
Phase E	Utilization
Phase F	Disposal

1.2.2 Mission Description and Goals

In recent years the rate of satellite launches has increased exponentially, to the extent that the number of active satellites orbiting around Earth has risen from approximately 1000 satellites in 2014 to around 6700 satellites in January 2023, as reported by Union of Concerned Scientists Satellite Database [12, 13]. Future projections foresee a further increase in the next decades, especially in Low Earth Orbit (LEO). As the space traffic increases, so does the probability of collision between two objects and the number of space debris². They can originate from different sources, including a functioning satellite which becomes inactive or a collision between two operational satellites as well as with another orbital debris. A potential collision could result in a wide range of debris that will remain in orbit for years, posing a threat to operational satellites, since any damage could disrupt essential services provided to date by satellites, such as communications, Earth observation, internet access and navigation, on which our societies rely. Therefore, implementing mitigation strategies, such as improving Space Situational Awareness (SSA), has become progressively more important. Defined as "the knowledge and characterization of space objects and their operational environment to support safe, stable, and sustainable space activities." by the US Space Policy Directive [14], SSA is also an essential part of the EU Space Programme [15] and thus aims to avoid collision hazards and manage space traffic by tracking the positions and trajectories of objects. Of course small debris are the hardest to track and identify, and the same

²"Orbital debris, or space debris, shall mean any human-made space object orbiting Earth that no longer serves any useful purpose." [14]

is true for very small satellites, especially in early stages of rideshare missions, in the first weeks after the deployment from the launcher. While CubeSats have been successfully tracked thousands of times, and also single PocketQubes have been proven detectable, what would happen if even smaller satellites were launched or if a cluster of picosatellites were flown in formation has yet to be explored.

In this context, this novel TU Delft mission would be composed of multiple picosatellites. The specific architecture, that will be further discussed, could consist of a single satellite that, once in orbit, will be separated in two identical and independent satellites, or a big satellite that, once in a lower altitude orbit, will release a series of subsatellites with different form factors. Very small satellites have limited capabilities in terms of Precise Orbit Determination (POD) and extremely reduced radar and optical cross-sections, thus being at the edge of detection capabilities [16]. The uncertainty in their positions contributes to a high risk of collision (see Figure 1.5, from [17]), which should be avoided.

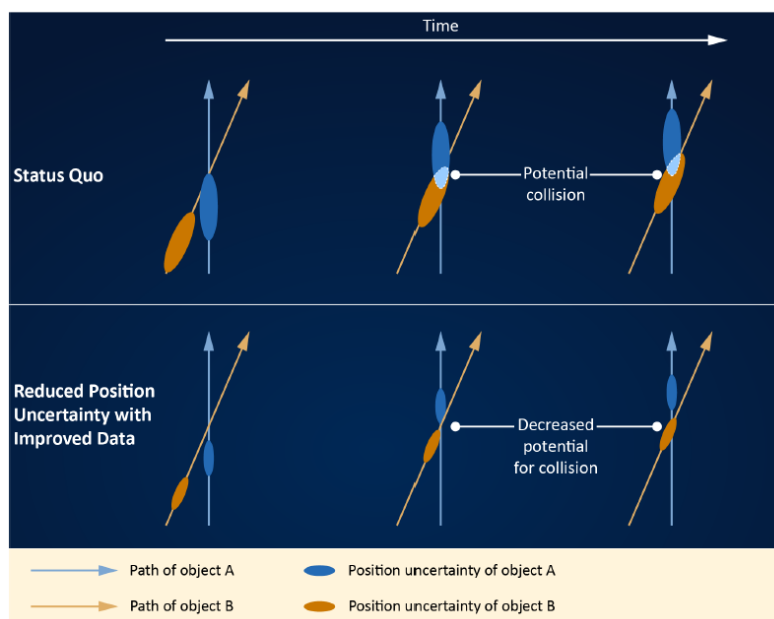


Fig. 1.5 The potential collision between two satellites would decrease if the uncertainty of satellite positioning was reduced. Source: GAO analysis of Department of Defense, National Oceanic and Atmospheric Administration, and The Aerospace Corporation images and information.

Therefore, the main mission goal is to evaluate tracking capabilities and limits of different sensors used for space situational awareness [16]. In addition, satellite

separation could also simulate the process of debris formation, providing a chance to have an indication of what is the current state of debris tracking performance by the SSA network. Ground-based tracking systems that will be used throughout this mission comprehend:

- Space Surveillance Radars;
- Laser tracking systems;
- Optical sensors and Telescopes;
- Radio transmissions;
- Spectro-polarimetric measurements.

Various space systems can be coupled with the ground network to improve the trackability of the satellites. For instance, there are on-board solutions which will increase their visibility, as Light-Emitting Diodes (LEDs), or provide satellite position data for validation compared to other systems, like the Global Navigation Satellite System (GNSS) receivers. Both will be included in TU Delft's satellites equipment. As for the former, these devices constitute an active source of illumination on the external surface of the satellites, which considerably enhances the trackability because it allows spacecrafts to be tracked also during eclipse period, providing a wider set of opportunities in which satellites can be observed [18, 19]. This concept has already been demonstrated by a successfully tracked high-altitude balloon equipped with LEDs and built as prototype for the LEDSAT mission, developed by Sapienza University of Rome. However, the long-term performances of LEDs is still unknown, and their degradation due to radiation exposure will require an extensive testing campaign before implementing them in future missions. On the other hand, GNSS receivers will serve as a mean to collect precise on-board navigation solutions data, and to provide accurate orbital elements too. Each subsatellite will carry its own receiver, thus being independent in orbital element determination. Their independence will be important especially in the case of a possible conjunction³, when GNSS data could be used to validate conjunction prediction algorithms.

In summary, the mission goals would be [16]:

³"A satellite conjunction is an event in which two satellites or a satellite and a piece of debris are estimated to pass near each other." [20]

1. Demonstrate in-space precise tracking of multiple pico- and femto-satellites down to accuracies better than what currently achievable with publicly available TLEs.
2. Demonstrate ground tracking (by means of radar, optical and laser tracking) of femto-satellites and assess the achievable orbital elements accuracies.
3. Test in-space identification of space objects using laser and optical instruments.
4. Provide independent position measurements for two objects involved in a conjunction.

Moreover, the mission lifetime will depend on different variables, as the altitude of the orbit and the size of the satellites. Keeping into account that the vast majority of commercial launches is at an altitude of 500 km and ensuring compliance with end-of-life disposal guidelines [21], a trade-off will be carried out in order to guarantee at least some months of test in orbit.

1.2.3 Project Timeline

As for 2023, the project timeline foresees the mission definition, with the investigation of payload prototypes and their mission requirements, and the definition of the satellite architecture. Also, the heritage of Delfi-PQ is exploited for improving the bus design. In 2024, the payloads will be selected and their design will be finalized in order to build a Flight Model, while finally the satellite integration and environmental tests will anticipate the launch no earlier than 2025.

1.2.4 Mission Architecture and Payloads

The final mission concept is not yet defined and, as of today, it oscillates between two extremes which will be further investigated in high-level mission analysis. The Extreme A includes a twin-satellite formation, specifically two identical 3P PocketQubes. The satellites would be launched docked together and, once in LEO, they will be detached. The Extreme B, instead, comprehends one major satellite, most likely a 3U CubeSat, that will deploy a cluster of satellites. The combinations of small satellites could be various and their release could be commanded on multiple

levels: at first stage 2U and 1U CubeSats or a 2x 1.5U CubeSats, which could contain 3P PocketQube, 1.5P PocketQube or even smaller picosatellites to deploy. The ultimate choice between the two should keep into account the results derived from the mission analysis, in addition to risk analyses and budget considerations.

For each satellite the core bus will be built exploiting re-use heritage from Delfi-PQ. Most notably, the core-bus will be composed of the following subsystems:

- Electrical Power System (EPS)
- Command and Data Handling System (CDH)
- Communication System (COMM)

On the other side, the satellites will carry different payloads which reflect the different tracking means. These payloads can be active, requiring energy to operate, or completely passive. Their prototype baseline, still subject to possible changes, is shown and briefly explained in Table 1.4.

Table 1.4 Mission Payloads.

Payload	Active (A) or Passive (P)	Objective
LEDs	A	To maximize visibility and improve detectability
Miniaturized GNSS Receiver	A	To determine the satellite position and velocity
Camera	A	For Space Surveillance and Tracking
Radiation Sensors	A/P	For on-board radiation monitoring
Laser Retro-Reflectors	P	To enhance laser ranging systems trackability
Optical Coating	P	To maximize visibility and improve detectability
Satellite License Plate	P	For satellite optical identification

The satellites will not be equipped with thrusters for attitude control, nor will they have an actual attitude determination and control system (ADCS), although plans are being made to use a miniaturized ADCS sensor as an additional payload for technology demonstration. Therefore, the satellites will be subject to random rotations along their three axes, and the only way to control their position will be to act on changing their drag area, such as by extending a solar panel.

1.3 Research Framework and Goals

In the scope of this thesis, it was decided to perform a high-level mission analysis focusing on one of the possible mission architectures mentioned above. Extreme A was chosen and, therefore, the core of the space segment will feature two identical and independent 3P PocketQubes. For this reason, the space mission object covered by this thesis will be also referred to as "TwinSat Mission".

1.3.1 Satellite in-Flight Separation and Control via Differential-Drag

The satellites will be launched as a single spacecraft. Once in orbit, their separation, which will occur through the use of separation springs, will kick off their flight in formation. The main objective of the mission analysis is to study this scenario in order to be able to investigate different topics and answer to the following questions:

- What are the safest direction of separation and detachment angle?
This study is needed to ensure collision avoidance of the two satellites, particularly during the first close passages. A collision, indeed, would not only mark the failure of the mission, but would also worsen the space debris issue.
- What are plausible values of separation relative velocity? How fast the satellites will move away?
The initial and average relative velocities should guarantee that the satellites will remain in close proximity for an adequate amount of time, allowing communications even without a high gain antenna, typically mounted on larger spacecraft.
- What are the consequences of using differential drag to control the satellite and keep the formation? What is the impact on satellite lifetime?
The variations in drag area, achievable with active control (e.g. deployable solar arrays) can be used to regroup the satellites, exploring their conjunctions.

The answer to these questions will be clarified in the remainder of this thesis.

1.3.2 High-level Requirements Elicitation

The ultimate goal of the preliminary mission analysis is to find technical requirements that will support the development of the mission. At the beginning of this thesis, several starting requirements and constraints were already defined. They constituted an input for all the simulation performed and they are collected in Appendix A, which also include an explanation on requirements identifiers (ID), categories and verification methods. Following the analyses, the initial requirements will be complemented by new high-level requirements, which will be provided in Chapter 4 and Chapter 5 and summarised in Appendix A.

1.3.3 Payload High-Level Design: the GNSS Receiver

The focus on the GNSS receiver is explained by the fact that equipping a satellite with a receiver means providing another method to calculate the satellite's position in real time. Acquiring on-board navigation solutions, and correlating them with data provided by Two Line Elements (TLEs), is a crucial capability, especially when satellites orbit in close proximity or perform a conjunction. In addition, future satellites will exploit the GNSS signal to be identified immediately upon release, shortly after the Radio Frequency is turned on [22]. This will attempt to solve the lengthy process of spacecraft identification by TLEs when multiple nano- and pico-satellites are launched all at once from a deployer.

The author's goal is to find a possible space-capable GNSS receiver that consumes an acceptable amount of power relative to the total power available to the payloads, which should also be evaluated. At a later stage, once a suitable GNSS receiver has been identified, its accuracy in positioning measurements can be tested and its power consumption, a complex challenge for a PocketQube, can be verified.

1.3.4 Thesis Outline

The development of this thesis followed a temporal and logical flow which is reflected in the division into the following chapters, whose content is briefly explained.

- **Chapter 2** deals with the background of orbital mechanics required to understand what was pursued in the remainder of the thesis.
- **Chapter 3** will introduce the performed mission analysis by presenting the methodology used, focusing attention to the software setups.
- In **Chapter 4** the analyses will be shown and the simulation results will be commented on. Eventually, the high-level mission requirements will be identified and gathered in Appendix A.
- In **Chapter 5** the power analysis is performed to estimate the power available for payload functioning, before focusing on an in-depth study to define and test a possible GNSS receiver for the proposed mission.
- **Chapter 6** will summarise the thesis conclusions, drawing several recommendations for future iterations of mission design.

Chapter 2

The Basics of Orbital Mechanics

This chapter covers all the fundamental concepts of orbital mechanics used in this work. The motion of a satellite orbiting a generic orbit can be described by several reference systems, some of which will be presented here. The coordinate system used to describe the motion of satellites flying in formation will also be shown.

The two-body problem and the various perturbative accelerations included in the propagator used in this thesis will then be introduced, as they have fundamental importance in the study of satellite control by differential-drag.

Orbits will be described in terms of classical, or Keplerian, orbital elements and, eventually, some basic orbital maneuvers will be studied, the effects of which will be useful in explaining some points of this thesis.

2.1 Reference Frames and Coordinate Systems

2.1.1 Earth-Centered Inertial Reference Frame

The Earth-Centered Inertial (ECI) Reference Frame is used to describe the orbital motion of a spacecraft in space relative to the Earth. As its name suggests, it is an inertial reference frame, meaning that it does not rotate with the Earth, but it remains fixed with respect to the stars.

The reference frame is shown in 2.1 and is defined by its origin and axes as follows:

- The origin, \mathbf{O}_{ECI} , is located at the Earth's center.

- \mathbf{X}_{ECI} points toward the Vernal Equinox, that is the intersection of the celestial equator and the ecliptic plane.
- \mathbf{Z}_{ECI} points toward the North Pole, being normal to the equatorial plane.
- \mathbf{Y}_{ECI} lies in the equatorial plane, completing the right-handed tern.

Due to Earth precession and nutation, the vernal equinox, the equatorial plane of the Earth, and the ecliptic plane vary. For this reason, to correctly define an ECI reference frame, a particular epoch should also be specified. In this work, the J2000 ECI Reference Frame will be used, which is based on Earth's position on January 1st 2000 at 12:00:00, and allows a mean reference equator and mean reference equinox to be defined.

2.1.2 Earth-Centered Earth-Fixed Reference Frame

The Earth-Centered Earth-Fixed (ECEF) Reference Frame is used primarily to describe the motion of an object on the Earth surface. In contrast to the ECI reference frame, it is not inertial but rather accelerated. It is fixed to Earth and rotates along with it with respect to the stars. The rotating angular velocity is equal to $\omega \sim 7.29218 \times 10^{-5}$ rad/s.

The reference frame is shown in 2.1 and is defined by its origin and axes as follows:

- The origin, \mathbf{O}_{ECEF} , coincides with the Earth's center.
- \mathbf{X}_{ECEF} points toward the Earth's prime meridian (Greenwich Meridian), lying in the equatorial plane.
- \mathbf{Z}_{ECEF} points toward the North Pole, being normal to the equatorial plane. It coincides with the Earth's rotation axis and overlaps with the \mathbf{Z}_{ECI} axis.
- \mathbf{Y}_{ECEF} lies in the equatorial plane, completing the right-handed tern.

An example of such a frame is the World Geodetic System(WGS)84.

2.1.3 Radial In-Track Cross-Track Coordinate System

The Radial In-Track Cross-Track (RIC) Coordinate System is a local coordinate system relative that describes the motion of a satellite with respect to another satellite and not with respect to Earth. From the ground, the orbits of two spacecraft can be described using the state vectors¹ or Classical Orbital Elements (COEs) in geocentric coordinate system, and their relative positions can be evaluated from the difference of their position vectors [24]. Nevertheless, to analyze and control the relative motion between multiple satellites, a local coordinates system is needed. Therefore, in this thesis, the RIC system will be used to study the two satellites flying in close-proximity.

This coordinate system is also illustrated in 2.1 and is defined by its origin and axes as follows:

- The system is centered on one of the satellite's center of mass.
- The **R** vector points along the satellite position vector, r , with respect to the central body (e.g. Earth).
- The **I** vector points along the satellite velocity vector, assuming the orbit of the satellite be circular.
- The **C** vector is perpendicular to both the radial and in-track directions, completing the right-handed tern.

Considering the RIC coordinate system and defining one satellite as target and one as chaser, the Clohessy-Wiltshire-Hills equations [24] describe the motion of the chaser relative to the target in a two-body dynamics. However, they are valid only for circular orbit and no external forces except gravity are included. In this work, the Systems Tool Kit software (STK) was used to calculate the trajectories and RIC coordinates of the satellites, taking into account orbit perturbations such as atmospheric drag and solar radiation pressure, as will be explained in the next chapters.

¹"A state vector is a vector that comprises the six components of the position vector and the velocity vector of a satellite, at any given time." [23]

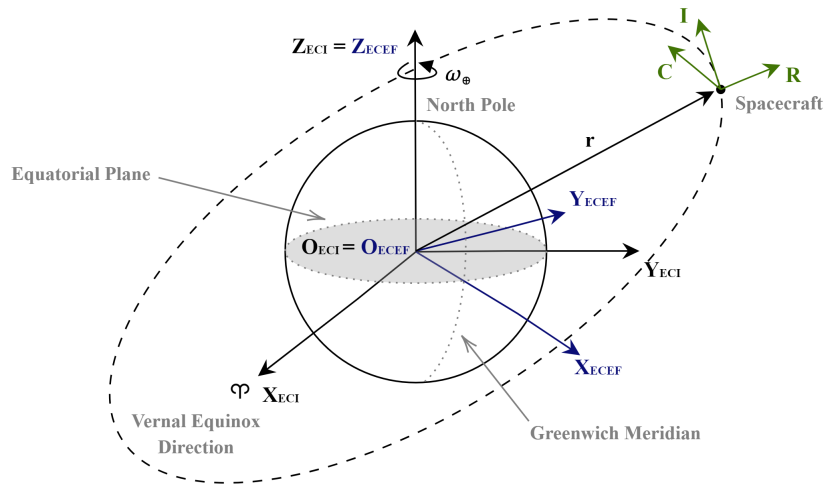


Fig. 2.1 ECI and ECEF Reference Frames; RIC Coordinate System.

2.2 The Two-Body Problem

The Two-Body Problem is a fundamental concept in orbital mechanics, which describes the motion of two celestial bodies under the unique influence of their gravitational attraction. The whole concept is presented in [24] in detail.

It is based on the following simplifying assumptions:

1. The bodies are treated as point masses, being considered to have spherical symmetry.
2. Gravitational force is the only force acting on bodies. All other external forces are neglected.
3. The mass of the secondary body (m) will be much less than that of the main body (M).

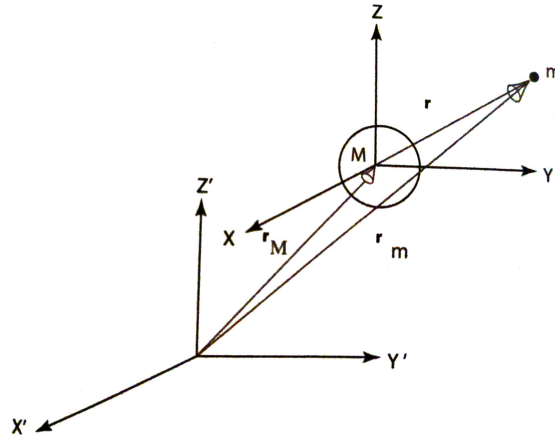


Fig. 2.2 The Two-Body Problem.

As shown in this graph taken from [24], an inertial reference frame ($\mathbf{X}', \mathbf{Y}', \mathbf{Z}'$) and a non-rotating set of coordinates ($\mathbf{X}, \mathbf{Y}, \mathbf{Z}$) parallel to the inertial frame and centered in mass M are considered. Furthermore, the position vectors of m and M are called respectively r_m and r_M , while their differences define the vector r as follows:

$$\mathbf{r} = \mathbf{r}_m - \mathbf{r}_M \quad (2.1)$$

It is demonstrated that applying Newton's motion laws and Law of Universal Gravitation is it possible to derive the vector differential equation of the relative motion for the two-body problem:

$$\ddot{\mathbf{r}} + \frac{\mu}{r^3} \mathbf{r} = 0 \quad (2.2)$$

where μ is the gravitational parameter, defined as the product of G , universal gravitational constant, and M , the mass of the central body:

$$\mu = GM = 3.986004418 \cdot 10^{14} \frac{m^3}{s^2} \quad (2.3)$$

By crossing the equation 2.2 into the specific angular momentum, \mathbf{h} , of a satellite and integrating it, is it possible to derive the trajectory equation which shows that the only possible path for an orbiting object in a two-body problem is a conic section (circle, ellipse, parabola, hyperbola), whose type determined by the constant e , eccentricity. Hence, considering a satellite as m and the Earth as its central body M , the equation 2.2 is the equation governing the state vector of the satellite orbiting around Earth.

Indeed, the equation includes \mathbf{r} , the position vector of the orbiting object relative to the center of the central body, and especially its time derivatives $\dot{\mathbf{r}} = \mathbf{v}$ and $\ddot{\mathbf{r}} = \mathbf{a}$, measured in the $\mathbf{X}, \mathbf{Y}, \mathbf{Z}$ non-rotating frame attached to the Earth. Thus, the state vector is defined as:

$$\begin{aligned}\mathbf{r} &= X\hat{\mathbf{I}} + Y\hat{\mathbf{J}} + Z\hat{\mathbf{K}} \\ \mathbf{v} &= v_x\hat{\mathbf{I}} + v_y\hat{\mathbf{J}} + v_z\hat{\mathbf{K}}\end{aligned}\tag{2.4}$$

where $\hat{\mathbf{I}}, \hat{\mathbf{J}}, \hat{\mathbf{K}}$ form a right-handed tern of unit vectors. By integrating the six components of the state vector, the state (\mathbf{r} and \mathbf{v}) at any time can be found. Also, a satellite state vector can be used to compute its classical orbital elements and vice versa.

2.3 Orbital Elements

In this thesis, to describe the characteristics of the initial orbit of the satellites and to pinpoint their position along the orbit, the six classical orbital elements were used. Five of them are sufficient to define the shape, size, and orientation of the orbit, while the sixth parameter allows one to specify the satellite's position along the orbit. The COEs (shown in Figure 2.3, adapted from [24]) are defined in [24] as follows:

- **Semi-major axis (a):** a constant defining the size of the conic orbit;
- **Eccentricity (e):** a constant defining the shape of the conic orbit;
- **Inclination (i):** the angle between the $\hat{\mathbf{K}}$ unit vector and the angular momentum vector \vec{h} ;
- **Longitude of the ascending node (Ω):** the angle, in the fundamental plane, between the $\hat{\mathbf{I}}$ unit vector and the point where the spacecraft crosses through the fundamental plane in a northerly direction (ascending node) measured counterclockwise when viewed from the north side of the fundamental plane. This angle is also known as Right Ascension of the Ascending Node (RAAN) angle;
- **Argument of periapsis (ω):** the angle, in the plan of the satellite's orbit, between the ascending node and the periapsis point, measured in the direction of the satellite's motion;

- **True anomaly at epoch (v_0):** the angle, in the plane of the spacecraft's orbit, between periapsis and the position of the satellite at a particular time, t , called the "epoch".

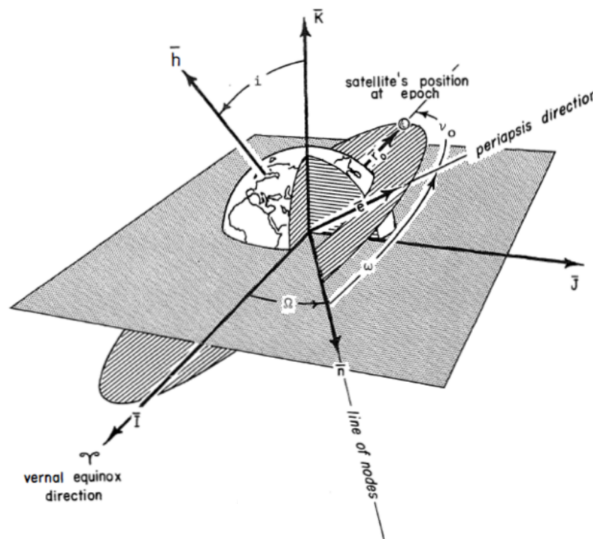


Fig. 2.3 Classical Orbital Elements.

The classical orbital elements are often referred to as Keplerian elements because they can describe a Keplerian orbit, based on Johannes Kepler's laws of planetary motion. Keplerian orbits are solutions of the two-body problem and, therefore, derive from the simplifying assumptions mentioned in section 2.2. However, there are some effects that cause deviation from the expected motion of the ideal Keplerian orbits. These effects, known as perturbations, will be introduced in the next section.

2.4 Perturbative Accelerations

One of the simplest methods to include all the perturbations is the Cowell's method, a special perturbation² technique according to which the equation of motion, together with the perturbations, should be written and then integrated numerically.

²"Special perturbations are techniques which deal with the direct numerical integration of the equations of motion including all necessary perturbing accelerations" [24]

Equation 2.2 becomes:

$$\ddot{\mathbf{r}} + \frac{\mu}{r^3} \mathbf{r} = \mathbf{a}_p \quad (2.5)$$

which, for numerical integration, would be reduced to the following equations:

$$\begin{aligned} \dot{\mathbf{r}} &= \mathbf{v} \\ \dot{\mathbf{v}} &= \mathbf{a}_p - \frac{\mu}{r^3} \mathbf{r} \end{aligned} \quad (2.6)$$

where \mathbf{a}_p is the term which comprehends all the perturbing accelerations. Some of the most important perturbations, taken into account by STK High Precision Orbital Propagator (HPOP), are now introduced.

2.4.1 Atmospheric Drag

For a satellite in Earth orbit, atmospheric drag can act as a perturbing force, causing the acceleration represented by the following equation [25]:

$$a_D = -C_D \frac{A_D}{M} \frac{\rho V^2}{2} \quad (2.7)$$

where:

- C_D is the drag coefficient;
- A_D is the satellite cross-sectional area along velocity vector. It is also known as "Drag Area";
- M is the satellite mass;
- ρ is the atmosphere density;
- V is the satellite speed relative to the atmosphere.

The minus sign denotes that the drag force acts in the opposite direction with respect to V . Equation 2.7 introduces an important parameter, $\frac{m}{C_D A_D}$, also called ballistic coefficient. The higher the ballistic coefficient, the longer the lifetime of a satellite. Indeed, as stated in [26], atmospheric drag reduces the energy of the orbit, causing secular decay in the semi-major axis and eccentricity, leading the satellite to lower altitude and higher-density regions of the atmosphere. More significant variations in

orbital lifetime due to changes of the cross-sectional area of the TU Delft mission satellites will be discussed in the thesis. Indeed, changes in drag area lead to different ballistic coefficient for two satellite in formation, causing differential drag. [27] Another important parameter in the drag term is the atmospheric density, which cannot be determined a-priori. Most notably, the density in a specific location is influenced by several factors, such as the day-night cycle, solar activity, Earth's magnetic field, and seasonal variations. The complexity of the prediction of the atmospheric density makes it challenging to correctly propagate the satellite and evaluate its lifetime. However, different models of atmospheric density have been developed, including the Jacchia-Roberts [28] model used in this work.

2.4.2 Solar Radiation Pressure

For a satellite orbiting Earth, the Sun causes a disturbance called solar radiation pressure. As stated in [23], this force derives from the transfer of momentum due to impact, reflection, absorption, and re-emission of photons. Such acceleration can be expressed as [25]:

$$a_R = -K C_R \frac{A_R}{M} \frac{L_S}{4\pi c r^2} \quad (2.8)$$

where:

- K is the fraction of the solar disk visible at satellite location;
- C_R is the coefficient for solar radiation. It is equal to $1 + \eta$, where η is the surface reflectivity;
- A_R is the satellite cross-sectional area normal to the Sun;
- M is the satellite mass;
- L_S is the luminosity of the Sun;
- c is the speed of light;
- r is the distance of the satellite from the Sun.

2.4.3 Third-Body Effects

The Moon and the Sun are considered point masses because the gravitational force they exert on the satellite is considerably weaker than that exerted by the Earth, given the distances involved. As a result, the magnitude of the perturbation caused by the presence of these third bodies is much smaller than the other perturbations involved. Therefore, the perturbative acceleration due to the presence of these third bodies is neglected.

Once the analytical formulation of the acceleration of the perturbation is defined, \mathbf{a}_p , the instantaneous position and velocity of the spacecraft can be calculated applying an integration method.

2.5 Orbital Maneuvers

An orbital maneuver refers to a change in the orbit of a satellite in space, in order to adjust satellite's position, velocity, altitude or inclination. To perform a finite thrust maneuver, a change in velocity is applied, quantified by a ΔV . On the other hand, a maneuver with an instantaneous change in the satellite's velocity is referred to as impulsive maneuver, which will be used in this thesis to model the spring force release.

For two satellites flying in formation, there are several types of maneuvers that can be performed, such as: station-keeping, relative orbit control, rendez-vous, collision avoidance, and others. The next section will introduce orbital maneuvering effects from a stable relative position, which are useful in explaining the orbital mechanics reasons behind the results of the analyses performed in this thesis.

2.5.1 Orbital Maneuvers from a Stable Relative Position and their Effects

If two satellites are in a stable relative position, it means that they are co-planar, at the same altitude and velocity, while they maintain their relative motion. On this basis, as explained in [29], different maneuvers, also referred to as "burns", can be given. They are listed below and shown in Figure 2.4, taken from [29].

- **Ahead (Prograde Burn) / Behind (Retrograde Burn).** Performing a prograde thrust (thrusting toward the target from behind it) will cause the chaser to initially approach, but then gain altitude and start falling behind the target. On the other hand, performing a retrograde thrust (thrusting toward the target from ahead of it) will cause initial movement towards it, but then orbital mechanics effects will cause the chaser to slow in its approaching velocity and start pulling away from the target. [29]
- **Radial In/Out Burn.** The inward radial thrust shifts perigee towards the burn point and create a sort of "football" orbit which first pulls ahead and then backwards. The outward radial thrust creates the same type of trajectory, but shifts the apogee toward the point of combustion. [29]
- **Out of Plane Burn.** An out-of-plane burn causes a slight tilt in the plane of the orbit. [29]

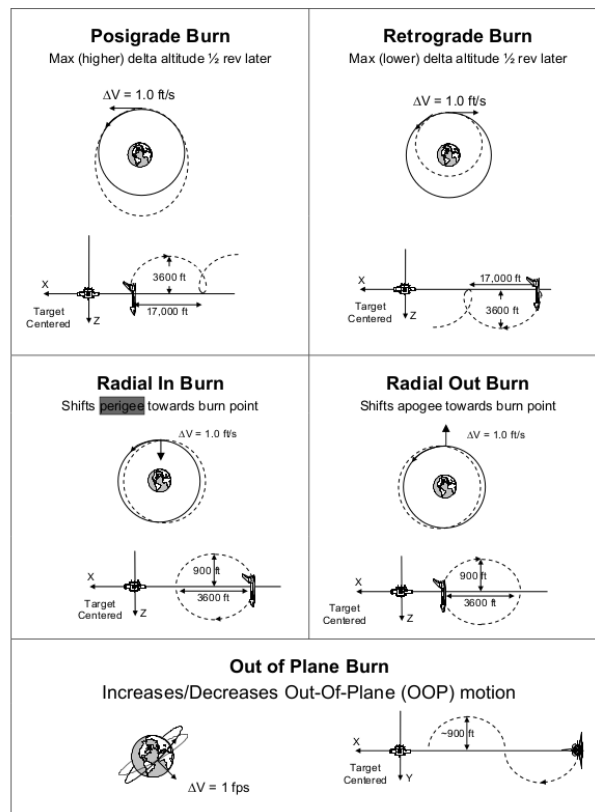


Fig. 2.4 Burns and Satellite Relative Motion.

In this thesis, some effects of these maneuvers will be of fundamental importance. To give an example, the spring force release for satellite separation will be modeled by an impulsive maneuver which will thus simulate prograde and retrograde burning for FirstQube and SecondQube respectively, while an increase in drag area will simulate a retrograde burn for the satellite under consideration.

Chapter 3

Mission Analysis

This chapter introduces the high-level mission analysis focusing on software settings. Different scenarios and mission control sequences were defined in STK, thus a thorough explanation of what lies behind each segment that builds the sequences can be found in the chapter. STK were integrated with MATLAB¹ to obtain most of the required analyses, therefore the interface between the two software will be discussed. Finally, ESA's Debris Risk Assessment and Mitigation Analysis (DRAMA²) suite is presented, as it was chosen to investigate the last simulation, concerning the orbital lifetime.

3.1 Scenario Definition and Implementation in STK

STK is a software that enables one to model complex systems that combine ground, sea, air and space assets, providing a realistic 3D simulation environment for digital mission engineering [30]. This tool is developed by Analytical Graphics Inc. (AGI).

For the purpose of this thesis, it was used extensively as the interaction between the system and component models allowed the author to measure the performance of this picosatellite mission. For each analysis shown in Chapter 4, a dedicated scenario was created. However, every scenario has several common features that will be introduced below. In particular, the STK Astrogator module, specialized in

¹Both STK and MATLAB could have been used thanks to the software license provided by Politecnico di Torino.

²DRAMA may be downloaded for free from ESA's Space Debris User Portal.

spacecraft mission planning, design, and analysis, was used. Astrogator also serves as one of the propagators available for a satellite object [31] and was selected among the others because it allows one to model in detail all the spacecraft maneuvers, taking into account an accurate orbital dynamics. Specifically, it enables the definition and execution of a Mission Control Sequence (MCS), which is a collection of all the operations, or Segments, to be performed by each satellite.

3.1.1 Analysis Period

Considering the mission timeline, which foresees a launch in 2025, it was decided to assume an analysis period with start time on 15 July 2025 at 12:00:00.000 UTCG³. The mission duration will be longer or shorter depending on the type of analysis, ranging from a few hours to a few months, and therefore it will be specified in each simulation.

3.1.2 Space and Ground Segments

"The Space Segment is part of the space system, placed in space, to fulfill space mission objectives" [33]. In the context of this dissertation, it refers to the two spacecraft, with their core buses and payloads. The space segment is composed of two 3P PocketQubes, named:

- **FirstQube**
- **SecondQube**

In STK, since a PocketQube model was not available, these satellites were inserted choosing a 3U CubeSat COLLADA (.dae) model for their visualization. Of course, all properties of the spacecraft were modified according to the properties of PocketQubes to be analyzed, as will be explained later. Each spacecraft was assigned as a reference vehicle to facilitate the calculation of relative motion values. No proper target or chaser will be defined, as the satellites will exchange these roles, chasing each other.

³UTCg refers to the Coordinated Universal Time date and time displayed in Gregorian format [32].

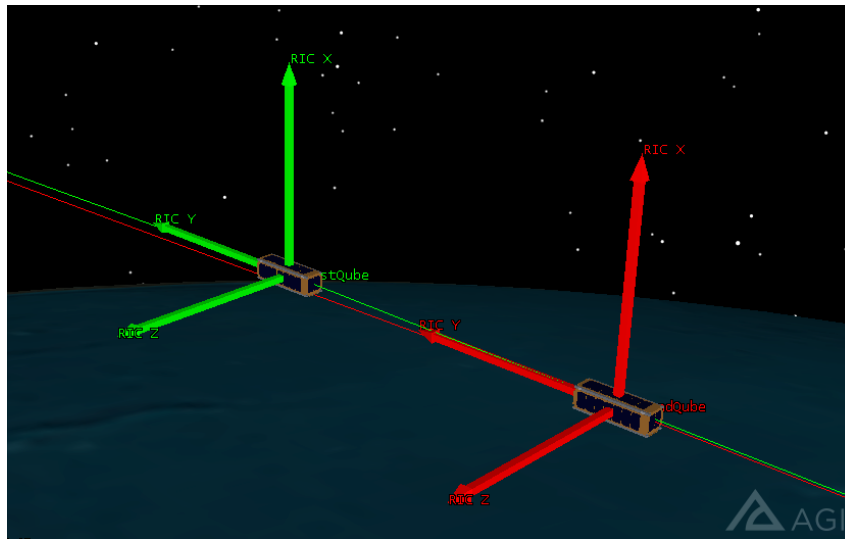


Fig. 3.1 FirstQube (green RIC axes) and SecondQube (red RIC axes) at the beginning of a scenario, shortly after their separation.

The ground segment is also part of the space system and typically includes all ground stations (GS) and the communication network needed to monitor and control the element of the space segment [33]. For this mission, several stations are to be considered to take into account optical, laser, radio or radar tracking. In this thesis, only two GS, the equipment for which is related to the TU Delft facilities, were added to the scenario:

- **Radio Ground Station.** It represents the GS located on the roof of the TU Delft - Faculty of Electrical Engineering, Mathematics and Computer Science building. In STK it was modeled with an isotropic antenna with a design frequency equal to 0.436 GHz.
- **Optical Ground Station.** In STK it was equipped with a "Simple Conic" sensor which has a 2-degree cone half angle, to model the Field of View (FOV) of a telescope for SSA tracking purposes that will soon be installed on the roof of TU Delft - Faculty of Aerospace Engineering building.

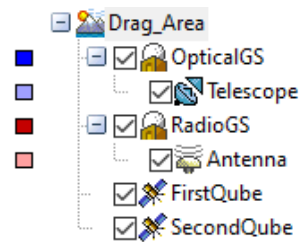


Fig. 3.2 Scenario Objects as defined in STK.

3.1.3 Satellite Control Sequences

Satellites ephemerides were computed by running the Mission Control Sequences, which were built in steps, based on the input requirements. A brief explanation of all segments of the Astrogator sequences and their characteristics follows.

- **Initial State (IS).** Their Initial State was defined in terms of orbital elements and spacecraft parameters. The satellites were placed in a circular and Sun-synchronous low Earth orbit at an altitude of 500 km. This value is due to a trade-off between the ideal orbital altitude for PocketQubes in circular orbits, which is below 400 km and would limit the orbital lifetime, decreasing the risk of creating a space debris [34], and the altitude of most commercial nanosatellite launches, which is in the range 500-550 km. Table 3.1 summarizes their common Keplerian elements, related to the initial orbit epoch that clearly corresponds to the start time of the analyses. The true anomaly ν was chosen such that the satellites have an initial offset, ensuring that they are exactly adjacent before their separation.

The Dry Mass was set at 0.545 kg, as provided by the Delfi Team. As discussed in Chapter 2, some of the key forces that influence orbital dynamics are the atmospheric drag, the solar radiation pressure, and also the thermal and albedo⁴ radiation pressure (RP), that led to the spacecraft parameters setting as shown in Table 3.2. The drag coefficient and the drag area values were also provided by the Delfi Team, which obtained them by fitting the satellite orbit decay using DRAMA.

- **Propagate (P).** These segments are characterized by the definition of the trajectory propagator and Stopping Conditions (SC), which establish where,

⁴In this case, albedo refers to the fraction of sunlight that is diffusely reflected by a Earth's surface.

Table 3.1 Orbital Elements of the spacecrafts.

a [km]	e	i [°]	RAAN [°]	ω [°]
6878.14	1.0E-4	97.5	0	0

Table 3.2 Spacecraft Parameters set in STK.

Drag		SRP (Spherical)		RP (Albedo/Thermal)	
C_d	Area [m ²]	C_r	Area [m ²]	C_k	Area [m ²]
2.2	0.02	1	0.02	1	0.02

when, or how trigger actions or end propagation.

To propagate the satellites objects, the Earth High-Precision Orbit Propagator (HPOP) Default v10 was used, which is a module responsible for numerically integrating the equations of motion to predict the satellites state vector as they move over time, in the J2000 reference frame. The numerical integrator used is the "RKF7th8th", i.e. the Runge-Kutta-Fehlberg method of seventh-eighth order, with a temporal step of 60 seconds. HPOP includes the following force models which were considered in the analyses: a gravitational field model (EGM2008), third-body gravity (Moon and Sun, both considered as point mass), solar radiation pressure, and atmospheric drag (Jacchia-Roberts Atmospheric Density Model). The drag model is set by default as spherical, as C_D and drag area were matched to the Delfi-PQ orbital decay.

As for the selection of Stopping Conditions, it was possible to choose in a wide spectrum of options, or even to customize one, thanks to the Component Browser, which contains a complete list of all components available in STK. In order to develop the mission sequences of interest, these conditions had to be used:

- Duration: Stop after a specified duration [35].
- Epoch: Stop on a specified date and time [35].
- Range (custom): Stop when the range between the two satellites reaches a specified value.

- **Maneuver (M)**. This segment allows one to select the type of maneuver to be executed, to set the attitude control parameters and the propulsion type. Our spacecraft will not have a proper ADCS or an engine that enables thrust vectoring, hence no actual maneuvers need to be implemented. However, at the beginning of the scenario, the two satellites, docked together, shall be separated by a spring force release. One way to simulate in STK the velocity given by the spring forces was to define an impulsive maneuver, providing thrust along the PocketQube RIC axes. The Cartesian tern $[X, Y, Z]$ or spherical coordinates [Azimuth, Elevation, Magnitude] were used to specify the direction of thrust, depending on what the analysis required.
- **Update (U)**. As the name suggests, this segment enables one to update the spacecraft parameters already set in the initial state. More in detail, it is possible to add or subtract a value to the preexisting one, or to set to a new value. The update option turned out to be really useful during most of the analyses, allowing one to easily increase or decrease the value of the drag area.

The most noteworthy analyses on close proximity operations have involved changes in the drag area, for which specific MCS, or algorithms, were defined. All of the earlier and simpler simulations were based on the steps required to arrive at these algorithms, and all of the subsequent ones used them to delve into other aspects. Therefore, the two main sequences will now be presented and commented on.

Sequence 1: Relative distance

This algorithm was built by controlling the satellite motion through stopping conditions based on their relative distance. First, the MCSs for FirstQube and SecondQube were defined in STK, and are highlighted in bold in Table 3.3. As some stopping conditions are based on relative motion, it was necessary to use MATLAB to run the simulations in multiple stages. Before describing the three fundamental steps, it is important to note that in STK each segment⁵ is characterized by an initial and final time.

1° Step: The trajectory of SecondQube is initialized by defining the initial state and performing an initial propagation of a few seconds. Afterward, the separation due to the release spring force is simulated, and the satellite is propagated until the stop time of the scenario.

2° Step: The trajectory of FirstQube is run. After defining the initial state and simulating the spring separation, the satellite propagates away from each other until it reaches a specific maximum distance. At this point, the drag area is instantaneously increased, and the satellite propagates approaching SecondQube until the point of minimum distance. The drag area is now decreased and the satellite propagates again to the distance marked as maximum, and then to the end-of-scenario epoch.

3° Step: Before starting the third and last run, the final time of the last propagation of FirstQube was extrapolated until the maximum distance, that is P_{4a} (see Table 3.3), and set it equal to the initial time of P_{2b} , that is the first propagation of SecondQube after separation. This means that, once the simulation has started and after the separation, SecondQube propagates freely until this particular time. Then, the drag area is increased and decreased, repeating the stages of the 2° Step, until the end of the scenario.

Therefore, as it was not possible to run the MCSs in steps only from STK's Astrogator suite, MATLAB was really helpful particularly to initialize the SecondQube trajectory and set a specific time that marks the time to stop propagating FirstQube and start propagating SecondQube. Moreover, as can be noted, in this case the most relevant stopping conditions act on the maximum and minimum distance, that is the

⁵The segments will be referred to as: Initial State (IS), Propagate (P), Maneuver (M), Update (U). Subscript a refers to FirstQube, while b to SecondQube.

Range between the two satellites, so when to vary the drag area is decided according to the relative distance.

Table 3.3 Mission Control Sequences. All the Stopping Conditions (SC) after the satellites separation are based on the relative distance.

FirstQube	SecondQube
	IS _b : Initial State
	P _{1b} : Until Duration SC
	M _b : Spring Force
	P _b : Until Epoch SC
IS_a: Initial State	
P_{1a}: Until Duration SC	
M_a: Spring Force	
P_{2a}: Until Max Range SC	
U_{1a}: Increase Drag Area	
P_{3a}: Until Min Range SC	
U_{2a}: Decrease Drag Area	
P_{4a}: Until Max Range SC	
P_{5a}: Until Epoch SC	
	$T_{P_{2b}}^{in} = T_{P_{4a}}^{fin}$
	IS_b: Initial State
	P_{1b}: Until Duration SC
	M_b: Spring Force
	P_{2b}: Until Max Range SC
	U_{1b}: Increase Drag Area
	P_{3b}: Until Min Range SC
	U_{2b}: Decrease Drag Area
	P_{4b}: Until Max Range SC
	P_{5b}: Until Epoch SC

The relative motion between the satellites (see Figures 3.3, 3.4) can be explained by the fact that both the impulsive maneuver associated with the spring force release and the increase in drag area simulate a retrograde burn mentioned in Chapter 2. In these cases, however, a retrograde thrust occurs in the opposite direction with respect to the target (and the direction of motion), when the chaser is behind the target. Hence, the chaser first moves away from the target for a brief period of time, and then approaches because it loses altitude and begins to accelerate. A conjunction is reached, and the chaser continues in its motion with higher velocity, until new actions are taken, such as decreasing the drag area of the chaser or increasing the drag area of the target, which will then become the new chaser.

The higher acceleration of the chaser is due to the fact that with a retrograde thrust the chaser will be in an elliptical orbit approaching perigee and, therefore, accelerating. This orbit has a smaller period than the original one, and so the chaser arrives at its

starting point somewhat earlier (see Figure 2.4) [29].

Obviously, decreasing the drag area has the opposite effect: a "prograde burn" will increase the altitude of the satellite under consideration, which will therefore slow down.

These orbital mechanics effect can be explained physically also through the conservation of mechanical energy (sum of kinetic and potential energy), which implies that if the satellite gains altitude it has to slow down, while if it loses altitude it has to speed up [24].

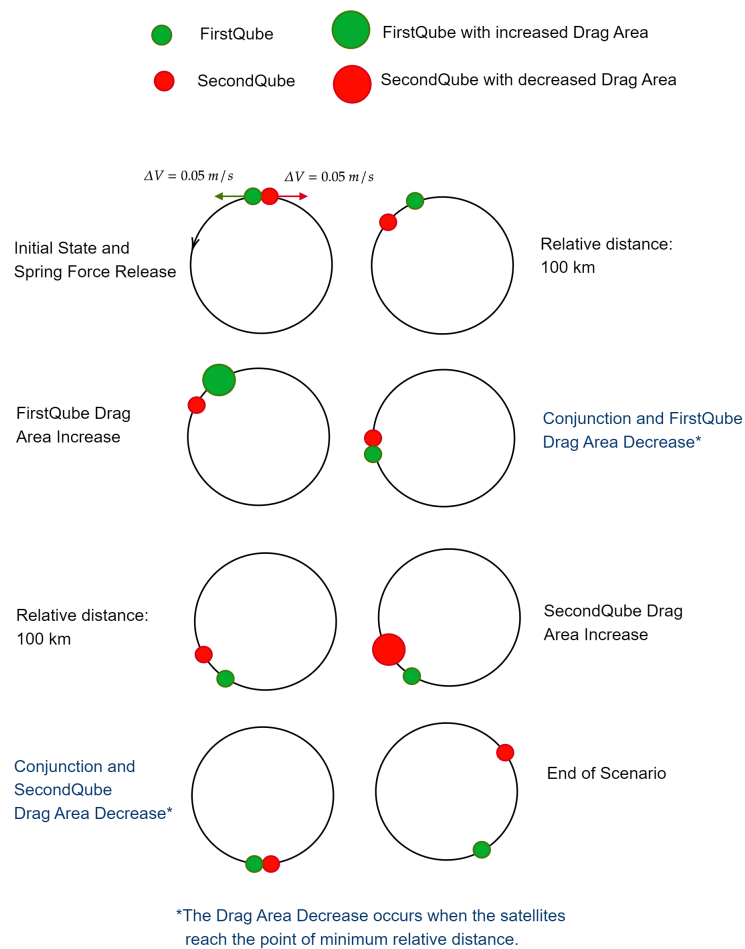


Fig. 3.3 This graphical representation (not to scale) is independent of time and actual orbits and is only intended to show the relative position of satellites as a result of changes to the drag area made during the implementation of a MCS with Sequence 1.

Sequence 2: Relative Distance and Relative Velocity

To improve the control strategy of the satellites, another sequence was created. This algorithm was built by controlling the satellites motion through stopping conditions based not only on their relative distance, but also on their relative velocity. The three phases into which the sequence is divided are now presented.

1° Step: The trajectory of SecondQube is initialized by defining the initial state and performing an initial propagation of a few seconds. Afterward, the separation due to the release spring force is simulated and the satellite is propagated until the stop time of the scenario.

2° Step: The trajectory of FirstQube is run. After defining the initial state and simulating the spring separation, the satellite propagates away from the other with a constant average and positive relative velocity, until it reaches a certain maximum distance, when the drag area is instantaneously increased. At this point, in this case, FirstQube does not directly propagate approaching SecondQube until the point of minimum distance, but it propagates in a high-drag configuration only for a limited period of time, that is, until its average relative approaching velocity is exactly opposite to the average velocity with which they were moving away. At that time, the drag area is decreased. FirstQube then propagates approaching SecondQube reaching first the point of minimum distance (on which no constraints have been set), then the point of maximum distance, and finally to the end of the scenario. To ensure the calculation of the time point at which the escaping relative velocity reaches a value opposite to the approach one ($T^{\text{avg.rel.vel}}$), this step is in turn carried out through two successive executions of the FirstQube MCS.

3° Step: Before starting the third and last run, it was extrapolated the final time of the last propagation of FirstQube until the maximum distance, that is P_{4a} (see Table 3.3), and set it equal to the initial time of P_{2b} , that is the first propagation of SecondQube after separation. This means that, once the simulation has started and after the separation, SecondQube propagates freely until this particular time. From this point on, the MCS is the same as that of FirstQube, with a short increase in drag area, before further propagation phases towards the end of the scenario.

Hence, now the stopping conditions act on the maximum distance and the relative velocity, which means that the control strategy is based on both the relative distance and the velocity between the two satellites.

Table 3.4 Mission Control Sequences. The Stopping Conditions (SC) after the satellites separation are based on both the relative distance and the relative velocity.

FirstQube	SecondQube
	IS _b : Initial State
	P _{1b} : Until Duration SC
	M _b : Spring Force
	P _b : Until Epoch SC
IS_a: Initial State	
P_{1a}: Until Duration SC	
M_a: Spring Force	
P_{2a}: Until Max Range SC	
U_{1a}: Increase Drag Area	
T_{P_{3a}}^{fin} = T_{avg.rel.vel}	
P_{3a}: Until Epoch SC	
U_{2a}: Decrease Drag Area	
P_{4a}: Until Min Range SC	
P_{5a}: Until Max Range SC	
P_{6a}: Until Epoch SC	
	T _{P_{2b}} ⁱⁿ = T _{P_{5a}} ^{fin}
	IS_b: Initial State
	P_{1b}: Until Duration SC
	M_b: Spring Force
	P_{2b}: Until Max Range SC
	U_{1b}: Increase Drag Area
	T_{P_{3b}}^{fin} = T_{avg.rel.vel}
	P_{3b}: Until Epoch SC
	U_{2b}: Decrease Drag Area
	U_{4b}: Until Min Range SC
	P_{5b}: Until Max Range SC
	P_{6b}: Until Epoch SC

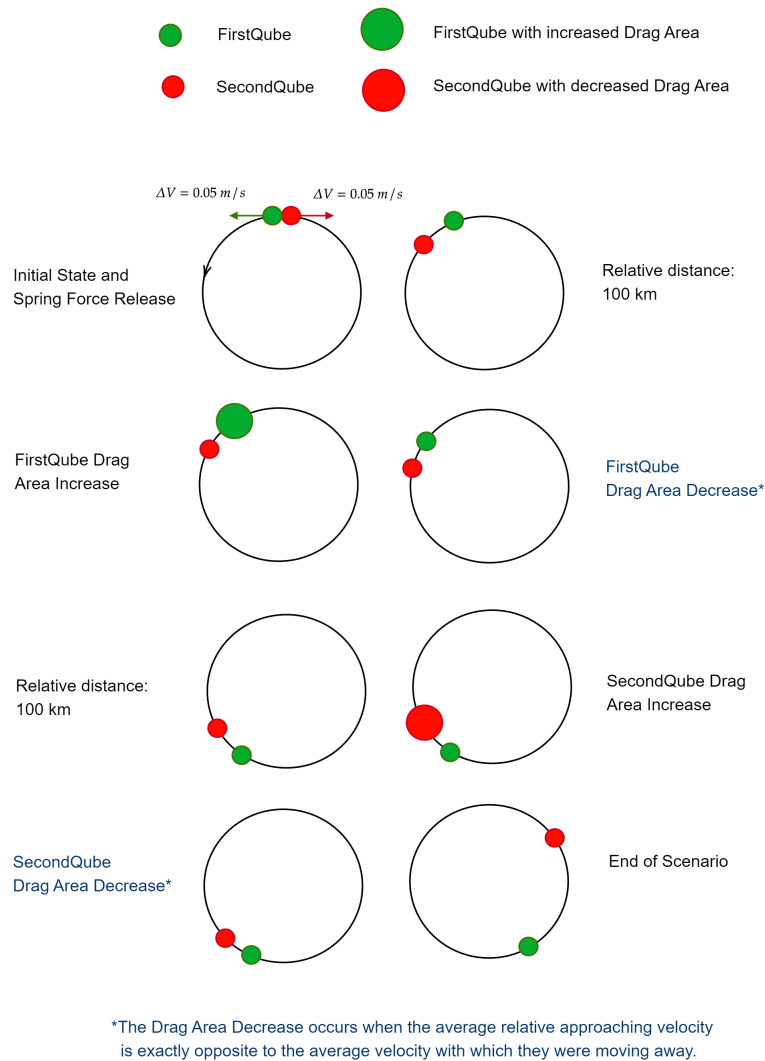


Fig. 3.4 This graphical representation (not to scale) is independent of time and actual orbits and is only intended to show the relative position of satellites as a result of changes to the drag area made during the implementation of a MCS with Sequence 2.

3.2 Integration with MATLAB

MATLAB is a high-level programming language and numeric computing environment, primarily used for data analysis, algorithms development, models and application creation. This software is developed by MathWorks.

It was possible to access and control STK from MATLAB using the STK Programming Interface [36], specifically the STK Object Model, which is an object-oriented interface and a collection of Microsoft COM (Component Object Model) libraries [37], including, among others, STK Astrogator. These libraries are made of different components (classes, interfaces, enumerations) that allowed to control the STK objects, to build custom solutions, and access the Data Providers Tools, to collect the datasets to generate reports or graphs. In particular, the integration of STK with MATLAB was crucial as it allowed the two MCSs to be executed in different steps and thus to be able to act on both satellites in the same simulation, as well as to easily iterate on different parameters and derive the corresponding graphs. In other words, the MATLAB interface was useful to automatize the process, editing scenario and objects' properties for trade study analysis, and to visualize large data sets from STK, exploiting MATLAB 2D and 3D plotting features. The interconnection between the two software suites for the purpose of this thesis can be explained through the following flowchart.

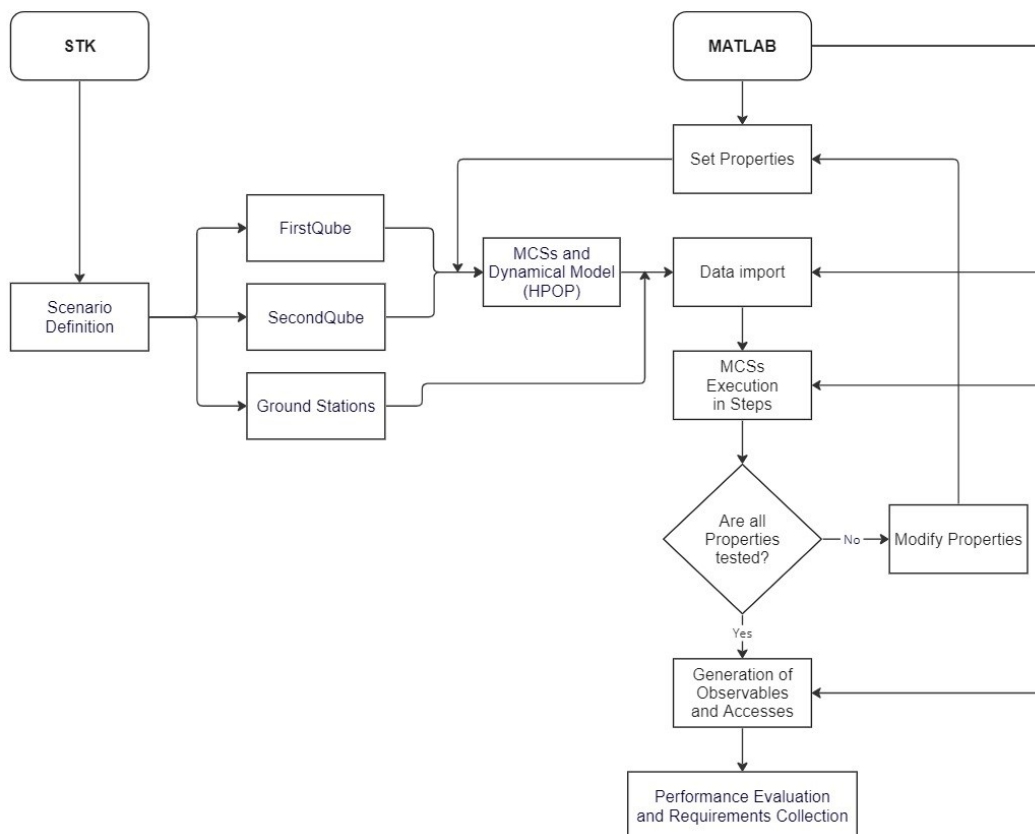


Fig. 3.5 STK and MATLAB interface in the context of this work.

3.3 DRAMA Tool Setup

DRAMA is a tool developed by ESA and a contractor team with the main goal to provide different analyses to ensure compliance of a space mission with space debris mitigation standards [38].

In the context of this thesis, it was used to assess the re-entry predictions for the satellites, in order to meet the requirement on the mission lifetime of at least 6 months (see Table A.3). To do that, two simulations with OSCAR (Orbital Spacecraft Active Removal) were launched: orbital elements and spacecraft parameters were first set, then an analysis of several disposal strategies (chemical or electric propulsion systems, electrodynamic tether or drag augmentation devices) was conducted, also considering future solar and geomagnetic activities for orbital predictions. The first simulation refers to a "Sequence 1" scenario, while the second simulation refers to a "Sequence 2" scenario. Therefore, both simulations are carried out inserting the same orbital elements, not selecting any disposal option, and taking into account Sun activity and geomagnetic predictions updated to September 2023. The main difference between the two scenarios are the spacecraft parameters and, in particular, the cross-sectional area value (i.e. drag area). Indeed, it might already be noted that one of the main differences between an MCS that provides stopping conditions based only on relative distance and an MCS for which they are based on both relative distance and relative velocity relates to the time the satellites spend in a high-drag or low-drag configuration.

DRAMA	
OSCAR - Orbital Spacecraft Active Removal	
Single Averaged Elements	
Semi-major axis / km	6878.1
Eccentricity / -	1.0E-6
Inclination / deg	97.5
Right asc. of asc. node / deg	0.0
Argument of perigee / deg	0.0
Mean anomaly / deg	0.0
Import Orbital States	
Spacecraft Parameters	
Cross-sectional area / m ²	<input type="text"/>  Open CROC
Mass / kg	0.5 Dry mass ▼
Drag coefficient	2.2
Reflectivity coefficient	1.3

Fig. 3.6 Orbital elements and spacecraft parameters in DRAMA

The simulations start on July 15th 2025, at 12:00:00 UTC. As for the orbital elements, they are the same as those set previously in STK. Similarly, the mass and the drag coefficient are given in Table 3.2. The reflectivity coefficient is set to 1.3 by default, while the cross-sectional area values will be calculated after the analyses in Chapter 4 and will therefore be shown later.

Chapter 4

Simulation Results and High-Level Requirements

The previously defined mission control sequences will be used in this chapter to analyze satellite in-flight separation in terms of release direction and velocity, while exploring the consequences of drag area variations. The results of a deployment angle study, carried out to define a limiting angle with respect to the direction of motion to avoid a collision on the first close passage after an orbit, are also shown. In addition, other analyses related to satellite ground station contact time and mission lifetime are included.

Throughout the various simulations, high-level mission requirements will be identified and listed in Appendix A.

4.1 Space Segment Analyses

Before introducing the results of the analyses, the reference system used is reported. It is a Radial In-Track Cross-Track reference frame centered on FirstQube, as shown in Figure 4.1. Furthermore, in all simulations, the satellite separation takes place on 15 July 15th 2025 at 12:00:05.000 UTC, which also corresponds to a separation occurring at the equator, with a latitude of 0.143 deg.

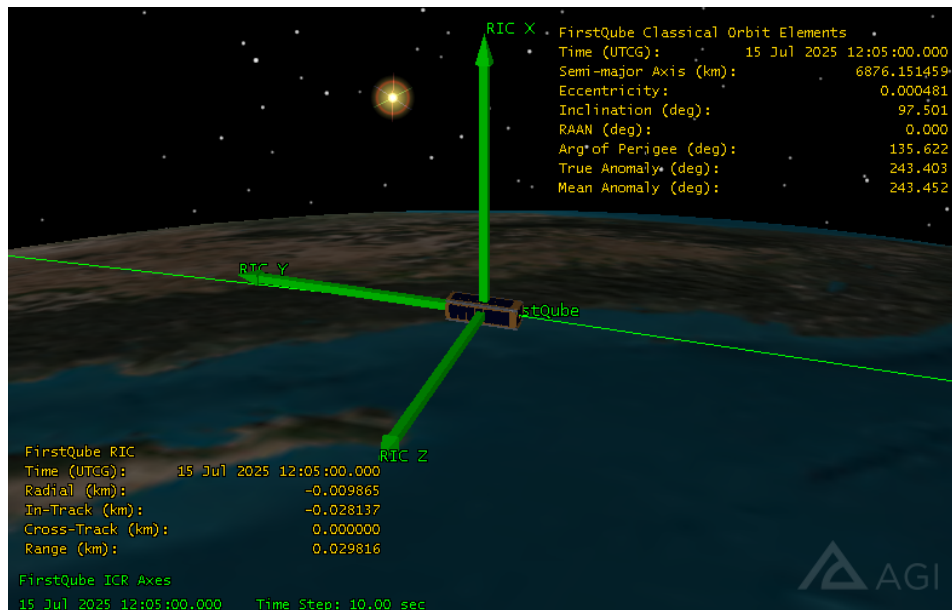


Fig. 4.1 RIC Reference Frame centered on FirstQube.

4.1.1 Direction of Separation

The first requirement to be investigated was the direction of separation of the two satellites. For this purpose, the satellites were released along each of the three directions of the RIC axes, trying to figure out which direction would avoid an impact between the two satellites in the short term.

Table 4.1 Initial MCSs for separation direction analysis.

FirstQube	SecondQube
IS_a: Initial State	IS_b: Initial State
P_{1a}: Until Duration SC	P_{1b}: Until Duration SC
M_a: Spring Force	M_b: Spring Force
P_{2a}: Until Epoch SC	P_{2b}: Until Epoch SC

The relative velocity due to the spring forces, hereafter also referred to as "separation velocity", had not yet been defined, hence it was chosen a plausible value of 10 cm/s, based on commercially available spring forces, according to a literature review [39, 40]. This implies that in STK FirstQube will perform an impulsive maneuver which provides a change in velocity of 5 cm/s along the thrust axis, while SecondQube will execute a maneuver of the same ΔV , on the same thrust axis, but with the opposite direction, thus -5 cm/s. The simple initial sequence, shown in Table 4.1, was built.

The period of analysis ranged from a few hours up to one month. For clarity, it should be mentioned that the graphs involving relative motion between satellites were obtained by extracting data from STK, specifically from the Data Providers "Astrogator Values - Relative Motion." For the calculation of relative distances or relative velocities, the reference point was considered FirstQube, which was assigned SecondQube as the reference object. In other words, as said before, the reference frame is a RIC system centered on FirstQube. The results are shown in the graphs below.

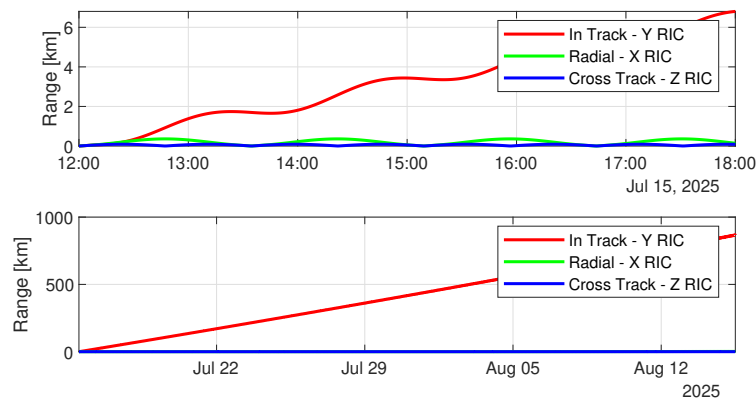


Fig. 4.2 Relative distance as a function of the direction of separation. Analysis periods: 6 hours, 1 month.

With respect to the directions considered, Figure 4.2 demonstrates that the separation direction which would increase the picosats safety would be along the velocity vector, i.e. the In-Track direction. In fact, by releasing the satellites in the Cross-Track or Radial direction, the satellites run multiple collision risks at the beginning of the scenario. Therefore, the result found can be turned into a recommendation:

*"The satellites **should** be separated along the In-Track direction."*

4.1.2 Separation Velocity

This analysis focuses on different separation velocity values, to evaluate the amount of time the two satellites can orbit in Close Proximity Operations (CPO): this encompasses a variety of activities that occur between two spacecraft in a relatively close area. The relative distance for CPO can vary depending on factors such as mission objectives, spacecraft capabilities, technology used, and safety considerations. This range extends from a few meters to tens of kilometers [41], and therefore in this mission the stopping limit condition was set at 100 km. The simulation was performed for different relative separation velocities, [5 10 20 30] cm/s, and the period of analysis lasted one week. The MCSs were the same as that used in the previous analysis, summarized by Table 4.1.

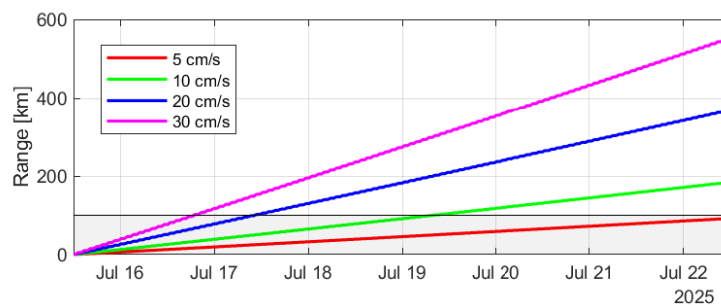


Fig. 4.3 Relative distance as a function of the increasing Separation Velocity. Analysis period: 1 week.

As can be seen, at a relative velocity of 10 cm/s, the satellites remain in proximity for about 4 days. It seemed a reasonable time span for CPO, compared to more than a week (for 5 cm/s) or less than 2 days (for [20 30] cm/s). Another recommendation follows:

*"The initial relative Separation Velocity **should** be equal to 10 cm/s."*

However, the choice of the separation spring force value needed a further confirmation. Therefore, next simulation, focused on the Drag Area changes, will iterate once more on the separation velocity value.

4.1.3 Drag Area Control: Stopping Conditions based on Relative Distance

Sequence 1 and the relative two MCSs reported in subsection 3.1.3 were constructed step-by-step and used in this analysis. Before showing the results, the values set in the "Range" stopping conditions and in the "Update" segments are introduced. Specifically, the stopping condition related to the maximum range of the satellites was set to 100 km (marked in the graphs), for the reasons explained above, while the stopping condition for the minimum range was set to 3 km, to ensure convergence of the algorithm. Instead, to find out the extent of the increase or decrease of the Drag Area¹, the simulation was performed for different increment factors: 2x, 3x, 4x. For the sake of clarity, a 2x increment means that a Drag Area of 0.02 m² would become 0.04 m², and similarly for other factors.

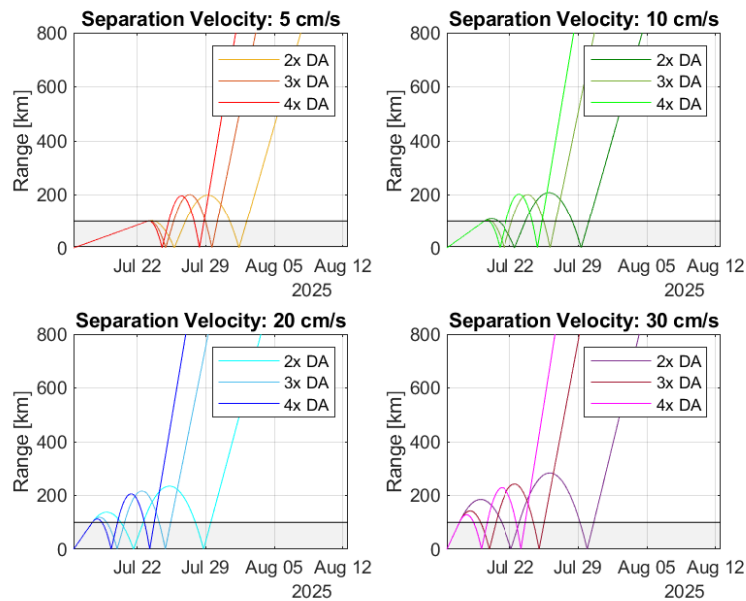


Fig. 4.4 Relative distance as a function of a fixed Separation Velocity and increasing Drag Area. Analysis period: 1 month.

This graph shows the range between the satellites over time, keeping the separation velocity fixed and increasing the Drag Area in each subplot. Running Sequence 1 allowed the Drag Area to be increased and decreased only once per satellite. This

¹"DA" stands for Drag Area.

also means once SecondQube reaches 100 km from FirstQube, the satellites are free to move away freely until the end of the simulation. The whole process creates overshoots, meaning the satellites move well over 100 km away before a new conjunction occurs. These overshoots, which should ideally be avoided, increase as the separation velocity increases. Furthermore, since satellites would move away faster and stay less time in close proximity, low initial relative velocity should be preferred. On the other hand, it is clear that the less the Drag Area would be increased, the more the satellites will orbit in close proximity. In addition, as shown in Figure 4.5, considering a 2x Drag Area factor, the relative velocity will oscillate in a lower range over time. As a result, it was chosen to continue the analyses taking into account an increase in Drag Area by a factor of two.

Assuming this, it can be seen that there are few differences iterating on the separation velocity values considered, both for the relative distance and velocity. As for the range between satellites, the second close passage occurs on August 1st for a velocity of 5 cm/s, while for all other higher velocities, it is always around July 28th-29th. Therefore, considering a preference for a low initial relative velocity for CPO purposes, and in the wake of previous simulations, it was established to set the relative separation velocity to 10 cm/s in further analyses.

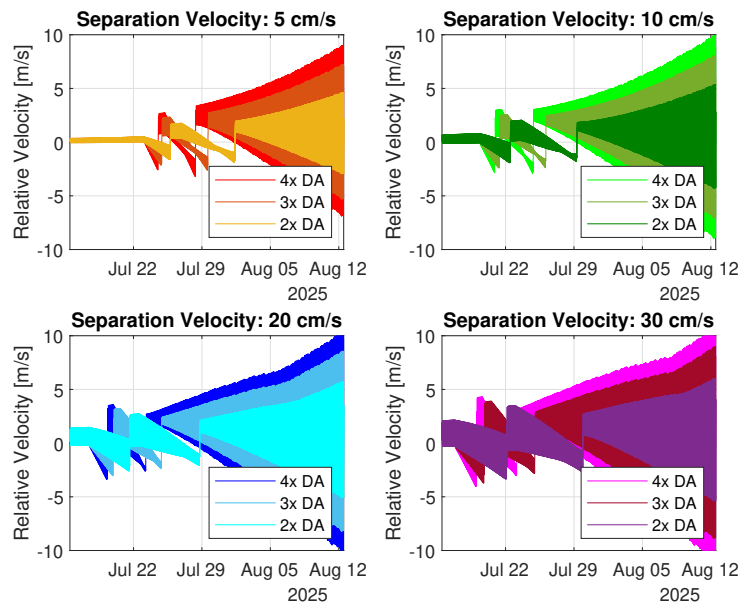


Fig. 4.5 Relative velocity as a function of a fixed Separation Velocity and increasing Drag Area. Analysis period: 1 month.

The increase in overshoots in the range graph and the smaller relative velocity fluctuations can also be verified by increasing the close passages between satellites. Indeed, a new sequence was built: it basically required Sequence 1 to be repeated three times. Again, for reasons of integration between STK and MATLAB, each time the propagation of some segments of a satellite sequence was started, it was necessary to exchange the final time of the last propagation of one satellite with the initial time of the upcoming propagation of the other.

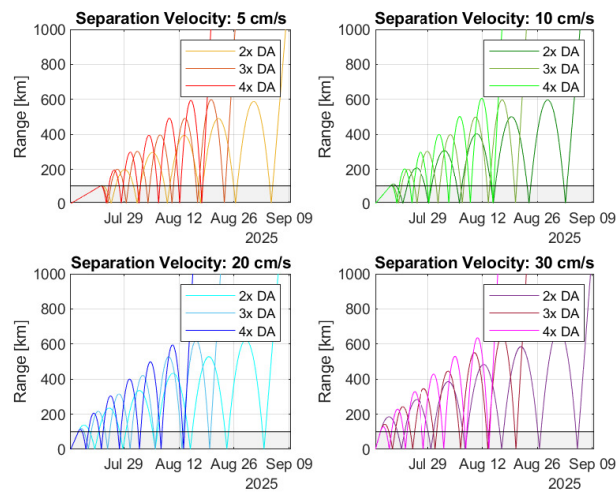


Fig. 4.6 Relative distance as a function of a fixed Separation Velocity and increasing Drag Area. Analysis period: 2 months.

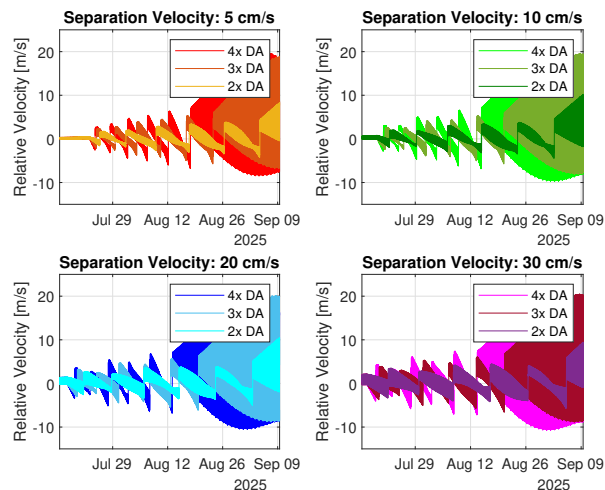


Fig. 4.7 Relative velocity as a function of a fixed Separation Velocity and increasing Drag Area. Analysis period: 2 months.

The results of this analysis led to the definition of two high-level requirements:

*"The initial relative Separation Velocity **shall** be equal to 10 cm/s."*

*"The Drag Area **shall** be increased and decreased by a factor of two."*

4.1.4 Drag Area Control: Stopping Conditions based on Relative Distance and Relative Velocity

Under the assumption that the satellites would orbit in the considered spatial range (within 100 km) for as long as possible, overshoots have to be controlled. One way to achieve this is for the satellites in the vicinity of conjunctions to move with an average relative velocity identical to the initial average relative velocity, achieved immediately after their separation. This objective would not be feasible with MCSs involving stopping conditions set only on range but, on the other hand, conditions placed on both range and relative velocity are needed. That is the main reason why Sequence 2, shown in Chapter 3, was built and used in the following simulation. A moving average filter was used to calculate the initial average velocity, thus the velocity at which to implement the decrease in Drag Area. Through the MATLAB command *movmean* [42], an array of local mean values of relative velocities is obtained. Each mean is computed over a sliding window of length equal to the average orbital period, across the neighboring elements of the relative velocity vector. In the reference orbit, the average orbital period was about 94 minutes, while the average initial velocity, considering a separation velocity of 10 cm/s, turned out to be approximately 30 cm/s. As mentioned above, the variation in Drag Area amounts to a factor of two. To present these results and better understand the differences, these graphs are overlaid with those of the previous analysis.

The relative distance between satellites, plotted hereafter, undergoes relevant changes due to the different MCSs, based on stopping conditions set only on range, or both range and velocity.

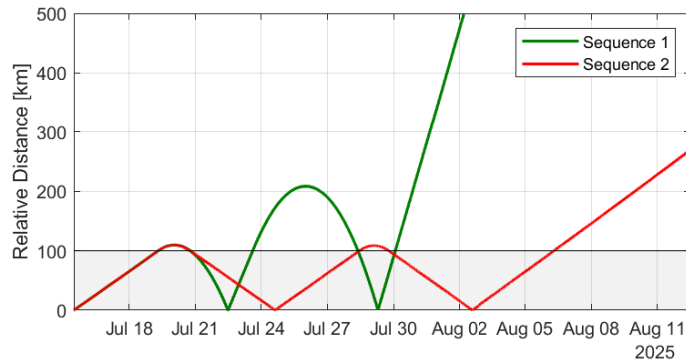


Fig. 4.8 Relative distance calculated with the two control strategies. Increase and decrease in Drag Area once per satellite. Period of analysis: 1 month.

It is clear that with mixed control over distance and velocity, overshoots can be limited. In fact, their magnitude does not exceed 110 km and does not increase with increasing close passages. Furthermore, the second conjunction calculated with Sequence 2 occurs more than 4 days after the one calculated with Sequence 1. As a consequence, the satellites spend more time in close proximity, even if only considering one change in Drag Area each. In principle, in the long term, it would be necessary to send commands to the satellite less frequently, considerably reducing the workload of the ground operators.

The following graphs highlight the differences in relative velocity and average relative velocity over the execution of the two Sequences. Averaging over the orbital period allows for almost complete smoothing of velocity fluctuations due to orbital dynamics.

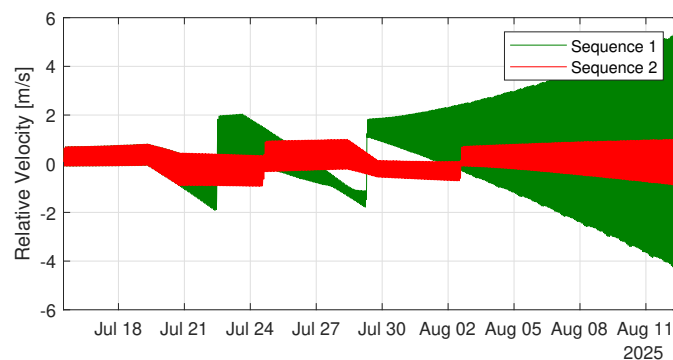


Fig. 4.9 Relative velocity calculated with the two control strategies. Increase and decrease in Drag Area once per satellite. Period of analysis: 1 month.

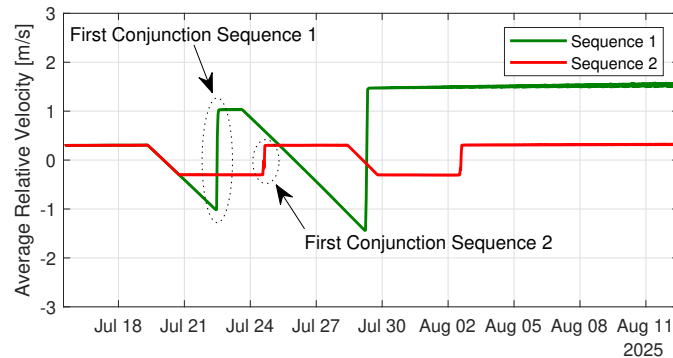


Fig. 4.10 Average relative velocity calculated with the two control strategies. Increase and decrease in Drag Area once per satellite. Period of analysis: 1 month.

From Figure 4.9 stands out that the velocity fluctuations are greatly reduced. For this reason the satellites are slower, and it is possible to make sure that in the conjunction neighborhood the satellites reach the relative velocity achieved after detachment by the release of the force of the separation springs. To verify that, Figure 4.10 enables to visualize the numerical value of average relative velocity at the first conjunction, which decreases in absolute value from 1 m/s to 30 cm/s.

It appears that in the time frame in which the conjunctions occur (highlighted in the graph), the relative velocity shifts from the negative value to the same positive value almost instantaneously. Actually, the velocity holds constant, and the sign change is due to the fact that the relative velocity takes into account the direction of motion. However, the change of sign, caused by the notation used, makes it possible to display the information about the satellites moving away, given by a positive relative velocity, or approaching, given by a negative relative velocity.

The comparison of the two implemented Sequences shows that the advantages of mixed control are numerous. These include a significant reduction in the time the satellite spends in high-drag configuration, which indicates the time span in which its Drag Area is increased. Considering only one variation (increase/decrease) per satellite, the average of the two time arcs in which FirstQube and SecondQube are in high-drag was calculated. Running the simulation with Sequence 1, this time arc is equal to 4.38 days, while with Sequence 2 it is 1.31 days. Therefore, already in the short term, the time span in which a higher Drag Area is needed is reduced by about 3 days. With control acting on both relative distance and relative velocity, the satellites would spend a long time in the same drag configuration, even with the same

attitude, which may be a disadvantage for scientific experiments to be conducted. However, less time in high drag conditions means also less braking and less loss of altitude, which would extend the satellite's life, providing more months of in orbit testing. To account for these results, a new requirement was formulated:

*"The Drag Area variations **shall** be managed by a control strategy that takes into account at least relative distance and relative velocity."*

Eventually, as before, a new simulation was started by increasing the number of close passages, constructing a new sequence based on repeating Sequence 2 to increase and decrease the Drag Area twice per satellite.

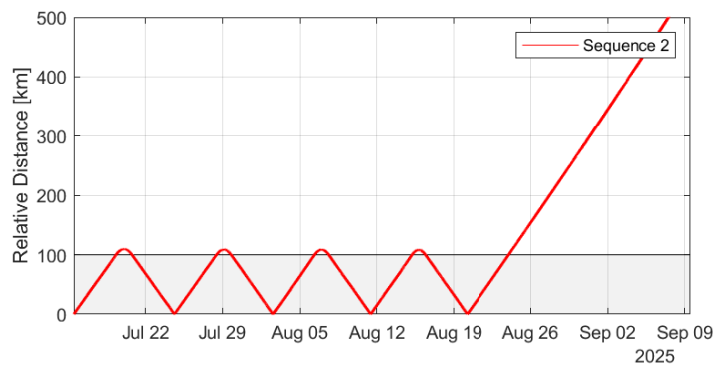


Fig. 4.11 Relative distance calculated with Sequence 2. Increase and decrease in Drag Area twice per satellite. Period of analysis: 2 months.

The tendency to reduce the velocity oscillations involved and have very low magnitude overshoots is confirmed. However, it should be noted that with the execution of Sequence 2 there are no stopping conditions related to the approach phase of the satellites, so there is no control over the minimum distance they reach during conjunction. As can be seen by zooming in on the minimum points, the relative distance decreases progressively, achieving a peak of 100 meters.

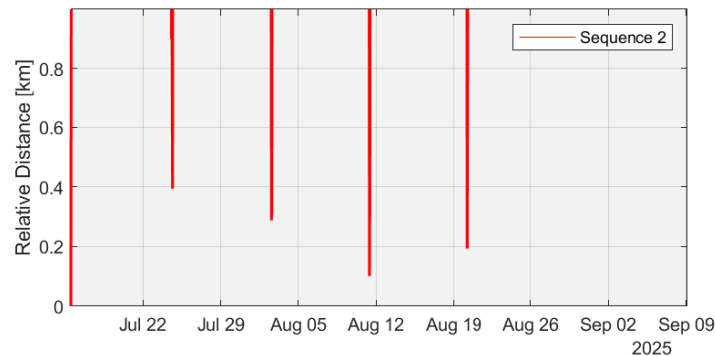


Fig. 4.12 Zoom in on points of minimum relative distance between satellites.

These values are far below the limit considered critical for collision risk, which is set at 1000 m. Typically, for any prediction of an approach under this edge, a warning flag is immediately sent to the spacecraft operator [43]. Therefore, it would be necessary to act on the Drag Area change even when the satellites are approaching, perhaps placing a new stopping condition. The consequences of new Drag Area changes are to be explored, although they would certainly adversely affect the frequency of sending commands to satellites.

4.1.5 Limiting Angle of Separation

Up to this point, all simulations have been carried out by performing satellite separation along the In-Track direction, which has proven to be the safest direction to avoid collisions. However, to account for the possible inability to stabilize the attitude and the presence of a satellite spin, it is worthwhile to check whether there are other directions in which it is safe to separate the satellites. For collision avoidance, indeed, it would be necessary to ensure that the satellites will be more than 1 km apart on their first and most riskiest close passage. Therefore, the author's goal is to find, if any, a limiting angle beyond which the satellites would surely impact.

Several simulations were carried out, detaching the satellites in different directions. Specifically, four types of analysis were performed:

1. Iteration over 14 Azimuth angles, spacing in the In-Track / Cross-Track (YZ) plane, with the Elevation angle equal to zero.

2. Iteration over 14 Elevation angles, spacing in the Radial / In-Track plane (XY), with the Azimuth angle equal to zero.
3. Fixing a given Elevation angle, iteration over 14 Azimuth angles, spacing from the Radial / In-Track (XY) plane towards the Radial / Cross-Track (XZ) plane.
4. Fixing a given Azimuth angle, iteration over 14 Elevation angles, spacing from the In-Track / Cross-Track (YZ) plane towards the Radial / Cross-Track (XZ) plane.

For the purpose of these simulations, it would have made no difference which Sequence to implement, given the emphasis on what occurs after at their close passage after only one first orbit, so in a very short period (around 94 min). Sequence 1 was used and consequently the orbital dynamics was the same as explained before, and the separation velocity was fixed to 10 cm/s. Furthermore, an attempt was made to change the separation latitude, by adding a propagation segment with a stopping condition set on the latitude reached before the satellites separation. It appeared that the change of latitude did not affect the calculation of the limiting angle, and thus the separation latitude has remained the same, at about 0 degrees, in all the simulations.

For FirstQube, azimuth and elevation angles are calculated from a reference system centered on the satellite's center of mass, and the same is done for SecondQube. These parameters are entered on STK in the maneuver segment, characterizing the impulsive maneuver in terms of spherical coordinates, specifically by introducing the azimuth, elevation and magnitude (Az, El, Mag) values taken in the STK reference system. In all simulations, the magnitude was always considered constant and equal to ± 5 cm/s, to account for the previously assumed relative separation velocity of 10 cm/s.

The conventions used to calculate azimuth and elevation, within the reference axis system, are presented. For simplicity, the reference frames shown are referred to FirstQube. The following view in STK highlights the triplet of axes and the angles convention, while the direction of motion is given by the positive direction of the Y axis.

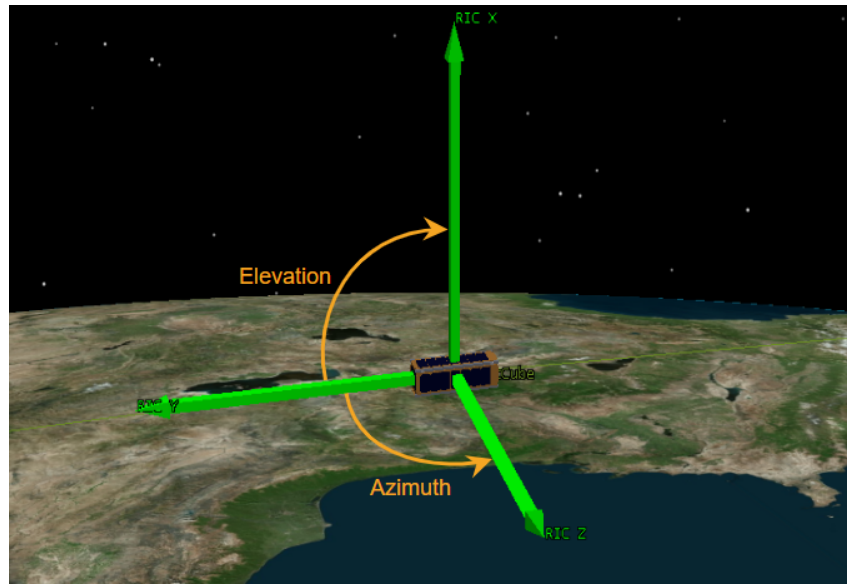


Fig. 4.13 Radial / In-Track / Cross-Track (XYZ) reference system centered on FirstQube, in STK. Azimuth (Az) and Elevation (El) angles are shown.

However, STK calculates these two angles differently, so two new figures are shown: the first one displays how STK calculates the angles; the second one illustrates the custom reference system used to calculate azimuth and elevation in the framework of this thesis, obtained by simply rotating the axes of Figure 4.13.

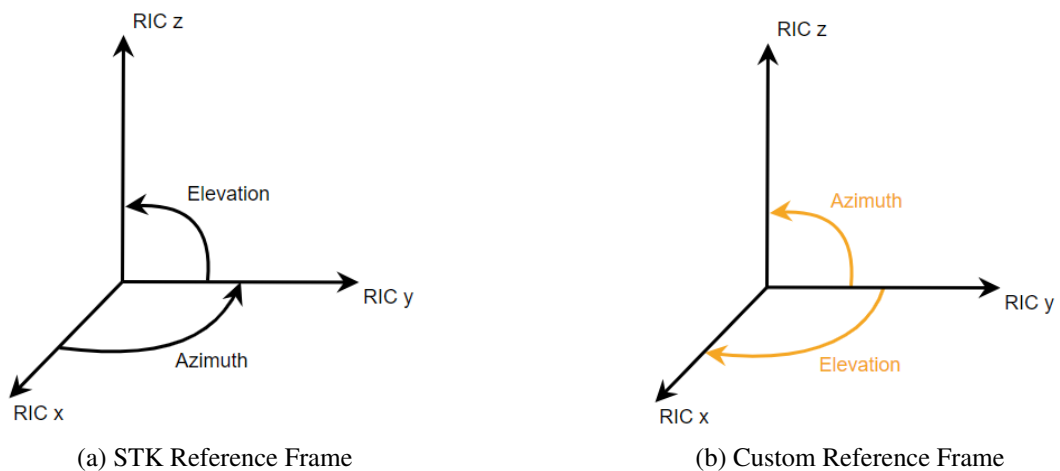


Fig. 4.14 Azimuth and Elevation angles shown in different Reference Frames.

The conversion factors used to switch from one system to the other are also given. They apply to the angles of azimuth and elevation for both satellites.

$$\begin{aligned}Az_{\text{custom}} &= El_{\text{stk}} \\El_{\text{custom}} &= 90 - Az_{\text{stk}}\end{aligned}$$

Finally, the vector of 14 angles, which can refer either to azimuth or elevation angles, is defined as follows:

$$[\text{angles}] = [0, 10, 15, 20, 30, 40, 45, 50, 60, 70, 75, 80, 85, 88]^\circ;$$

Simulation 1

The input parameters taken with respect to the custom reference system and used for this simulation are shown.

Table 4.2 Azimuth and Elevation angles for Simulation 1.

FirstQube	SecondQube
$El = 0^\circ$	$El = 180^\circ$
$Az = [\text{angles}]$	$Az = -[\text{angles}]$

Since there is no component of motion in the radial direction, this first graph shows what happens to the relative distance in In-Track / Cross-Track plane as the azimuth angle increases. At first glance, for angles up to about 50 degrees, there is a slight difference in the time the satellites take to move away up to 100 km. For higher angles, instead, the satellites take longer, maximizing the time they spend in close proximity. However, zooming in on the first orbit, Figure 4.16 shows that under a certain angle the relative distance of the satellites drops to less than 1 km on their first close approach (FCA).

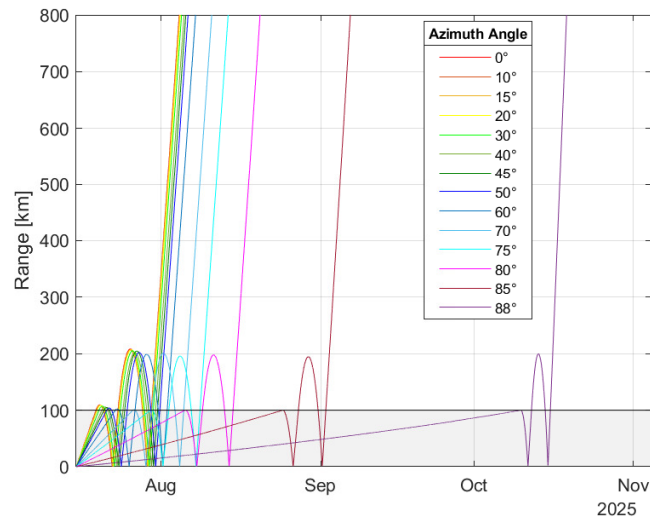


Fig. 4.15 Relative Distance over time, calculated for 14 Azimuth angles. The Elevation angle is equal to zero. Period of analysis: 4 months.

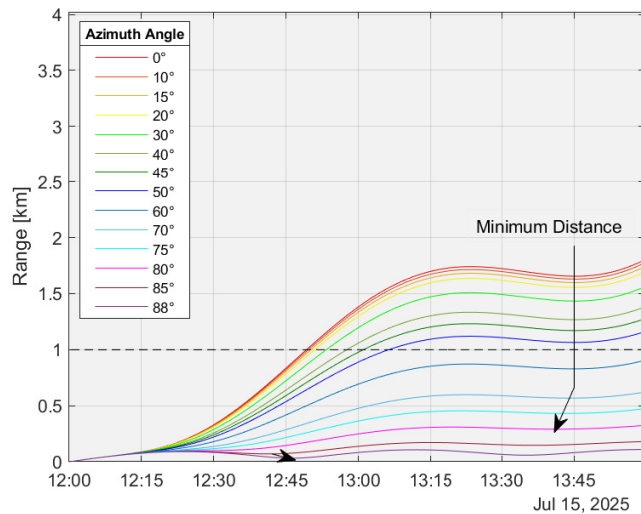


Fig. 4.16 Zoom on the first satellite orbit of Figure 4.15 to highlight the points of minimum distance.

The positive azimuth angles in the figures refer to those calculated for FirstQube. As for SecondQube, the resulting azimuth angle, i.e., its opposite (see Table 4.2), was considered in the calculations. To visualize more clearly the exact angle at which the transition over 1000 m occurs, another graph was created by plotting the minimum

distance versus the azimuth angle. In this case the limiting azimuth angle turned out to be 52.7°.

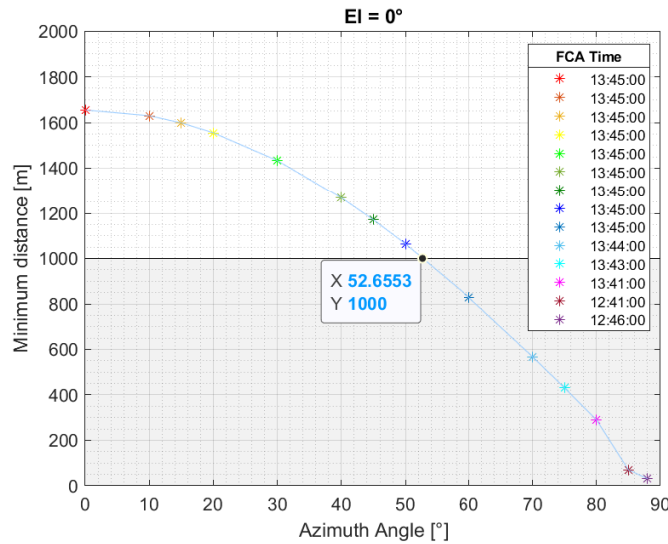


Fig. 4.17 Minimum distance as a function of the Azimuth Angle.

Simulation 2

The input parameters taken with respect to the custom reference system and used for this simulation are shown.

Table 4.3 Azimuth and Elevation angles for Simulation 2.

FirstQube	SecondQube
Az = 0°	Az = 0°
El = [angles]	El = 180° + [angles]

These graphs are analogous to the previous case, with the only difference that now there is no component of motion in the Cross-Track direction, while the iteration is done by spacing the elevation angle.

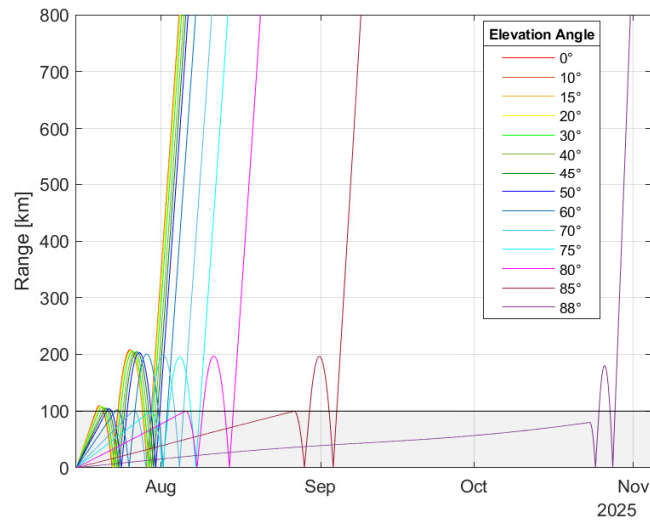


Fig. 4.18 Relative Distance over time, calculated for 14 Elevation angles, while the Azimuth angle is equal to zero. Period of analysis: 4 months.

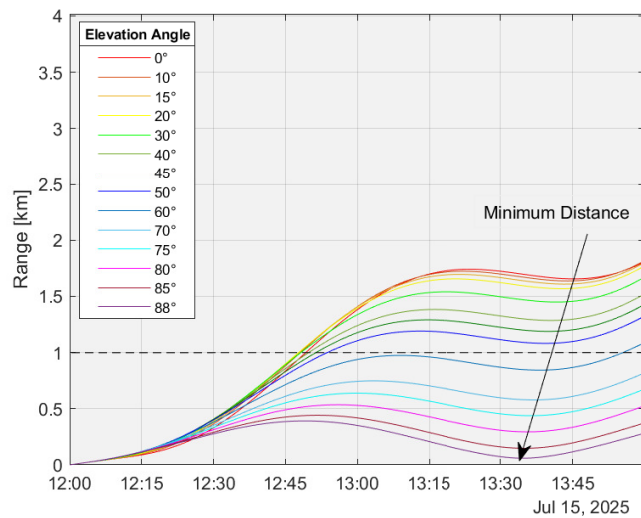


Fig. 4.19 Zoom in on the first satellite orbit to highlight the points of minimum distance. Period of analysis: 4 months.

The positive elevation angles in the figures refer to those calculated for FirstQube. As for SecondQube, the resulting elevation angle, shown in Table 4.3, was considered in the calculations.

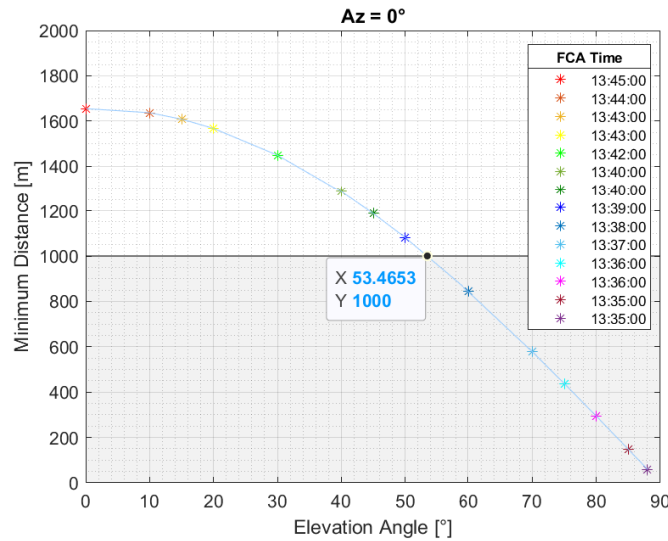


Fig. 4.20 Minimum distance as a function of the Elevation Angle.

In this case, the limiting elevation angle turns out to be 53.4°. Hence, the extremes that should not be exceeded with a separation in the In-Track / Cross-Track or In-Track / Radial plane have been found. The consequences of satellite separation carried out along other directions are investigated in the next simulations.

Simulations 3 and 4

By fixing an elevation angle and iterating over the 14 azimuth angles, simulation 3 was repeated for N=17 elevation values. The ultimate goal was still to search for the limiting angle beyond which the satellites would collide.

Table 4.4 Azimuth and Elevation angles for Simulation 3.

FirstQube	SecondQube
El = x	El = 180° + x
Az = [angles]	Az = -[angles]

The same process was performed by fixing an azimuth angle and iterating over the 14 elevation angles. Once again, the azimuth limit angle was found by repeating the simulation for N=17 times.

Table 4.5 Azimuth and Elevation angles for Simulation 4.

FirstQube	SecondQube
Az = x	Az = - x
El = [angles]	El = 180° + [angles]

The azimuth and elevation limit (*) angles which, for simplicity, are collected only for FirstQube, are summarized in the next table and then plotted in a 3D graph through MATLAB.

Table 4.6 Azimuth and Elevation Limit angles.

Simulation 3		Simulation 4	
El [°]	Az* [°]	Az [°]	El* [°]
0	52.7	0	53.4
5	52.6	5	53.2
10	52.2	10	52.7
13	51.8	13	52.3
15	51.4	15	51.9
20	50.3	20	50.7
25	48.6	25	49.0
30	46.3	30	46.5
35	43.1	35	43.3
40	38.8	40	38.7
45	32.4	45	32.1
50	22.0	50	21.0
51	19.0	51	17.4
52	15.1	52	12.3
52.5	12.3	52.5	7.10
53	8.40	53	does not exist
54	does not exist	54	does not exist

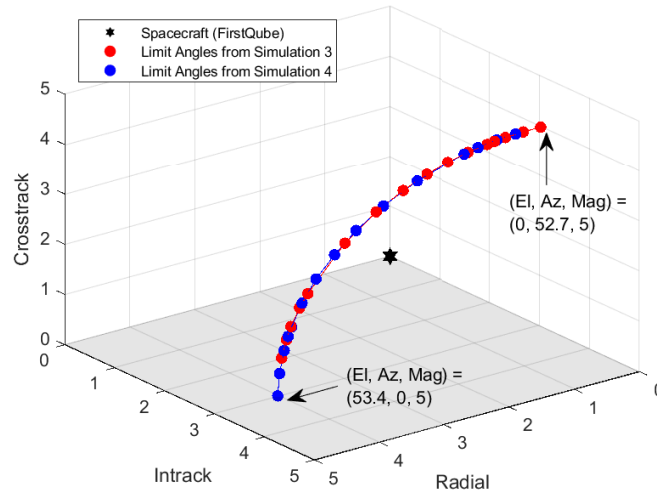


Fig. 4.21 Limiting Angles from Simulation 3 and 4.

It can be seen that the set of these points creates a curve in space. By joining these points at the satellite's center of mass and projecting them on the Radial / In-Track plane, a region of space is identified within which separating the satellites could be considered safe.

Since the ultimate goal was to evaluate the limiting angle with respect to the direction of motion, the projection of the (Az, El) coordinates (shown in Table 4.6) along that direction was calculated. The angle with respect to the direction of motion was calculated using the following formula:

$$\theta = \arcsin(\sqrt{\sin(Az)^2 + \sin(El)^2}) \quad (4.1)$$

For simulation-3 coordinates, it was found that:

$$\theta_{min} = 52.7^\circ \quad \theta_{max} = 63.7^\circ$$

while for simulation 4:

$$\theta_{min} = 53.4^\circ \quad \theta_{max} = 63.8^\circ$$

The global minimum defines the half-aperture angle of the cone, thus equal to:

$$\theta = 52.7^\circ$$

Furthermore, the effects of a separation in other symmetric directions should give similar results in terms of limit angles. Therefore, by mirroring the curve displayed in Figure 4.21 with respect to the different planes of symmetry, a cone is defined. Its vertex coincides with the satellite's center of mass, with a half-aperture angle of 52.7 degrees.

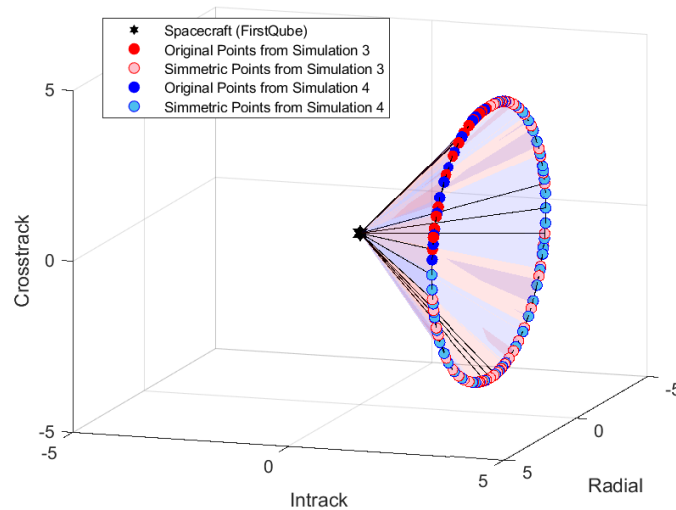


Fig. 4.22 The set of points that defines the region of space for which satellite separation leads to a relative distance greater than 1 km at the first close approach.

As a consequence of these last simulations, another technical requirement was established:

*"The satellite separation **shall** occur within the region of space bounded by a cone centered in one of the satellites center of mass and with a maximum half-aperture angle of 52.7°."*

4.2 Orbital Lifetime Variations

The objective of this analysis is to estimate the lifetime of the satellites, so as to verify that it guarantees at least 6 months of in-orbit testing. Focusing on one of the twin satellites, two simulations were run through DRAMA, each based on one of the two control "Sequence" of the satellites defined in Chapter 3 and that were then reflected in the different control strategies commented in the 4.1.3 and 4.1.4 analysis. The difference between the two simulations lies in the value of the cross-sectional area, which depends on the time the satellites spend in high-drag and low-drag configuration.

4.2.1 Simulation: Sequence 1

In this case, the stopping conditions are based only on the relative distance. As already calculated, considering one complete period (increase/decrease of drag area) per satellite, they are in a high-drag configuration for 4.38 days over a period of about 13.77 days, corresponding to a percentage of about 32%. This means that the satellites spend 32% of the time at 0.04 m^2 and the remaining 68% at 0.02 m^2 . Consequently, the average value of the drag area over an entire period is 0.0264 m^2 , which corresponds to the cross-sectional area value entered in DRAMA.

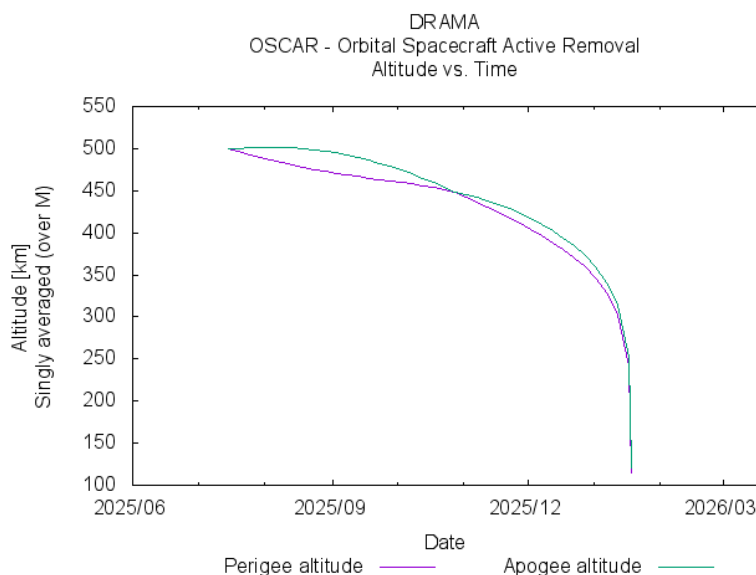


Fig. 4.23 Altitude vs. Time for Simulation 1

In the DRAMA - OSCAR report, the altitude-over-time graph shows that about 6 months of lifetime is guaranteed, thus meeting the mission lifetime requirements at the limit. However, the lifetime is expected to increase further with the next simulation.

4.2.2 Simulation: Sequence 2

The stopping conditions are based on both relative distance and relative velocity. Always considering one complete variation period per satellite, in this case the satellites spend 1.38 days in high-drag configuration over 14.28 days, corresponding to a much lower percentage of about 9.7%. Therefore, the satellites spend 9% of the time at 0.04 m^2 and the remaining 91% at 0.02 m^2 . Consequently, the average value of the drag area for an entire period is now 0.0219 m^2 .

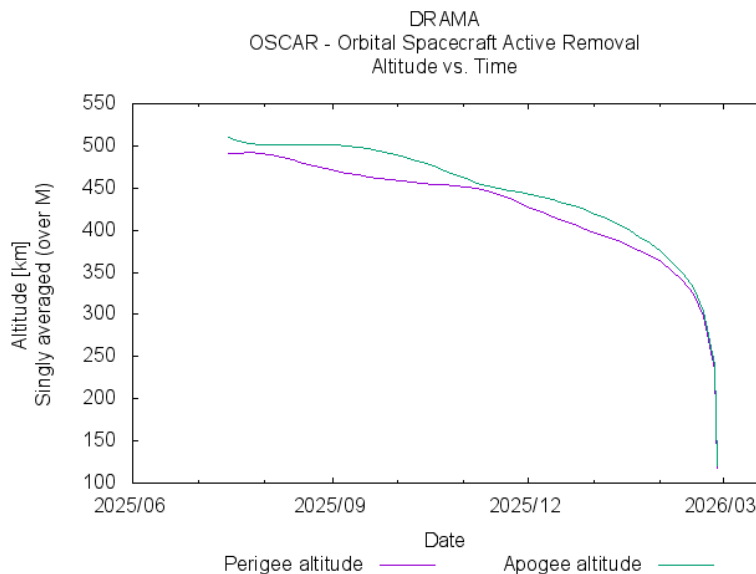


Fig. 4.24 Altitude vs. Time for Simulation 2

The graph of altitude-over-time shows 7.5 months of mission duration. In this simulation, 1.5 months were gained, providing a margin over the minimum duration of 6 months set by the requirement. With future improved control strategies, the mission duration could be further extended. Moreover, a launch from an altitude higher than 500 km could be considered, if the compliance with end-of-life disposal guidelines is ensured.

4.3 Accesses

Several analyses have been performed to verify if the scenario built ensured a minimum number of accesses between satellites and ground stations, thus fulfilling one of the mission goals. "Sequence 2", proved to be the most effective, was used in these analyses, providing as input an analysis period of one month.

4.3.1 Accesses between Satellites and Radio Ground Station

For the Azimuth-Elevation mask of the radio ground station, a constraint of 5 degrees of elevation was set to account for obstruction avoidance and interference reduction. The accesses were calculated for both FirstQube and SecondQube, showing little differences. In particular, for each satellite about 150 accesses (5 per day) were found, with a mean access duration of 7 minutes. Therefore, constant radio coverage was guaranteed.

4.3.2 Accesses between Satellites and Optical Ground Station

In this case, a constraint of 45 degrees of elevation was required (see Appendix A), to have less influence from atmospheric extinction and light pollution, two crucial factors in optical detectability. For satellite reflective detection, solar illumination is required. Therefore, two sunlight constraints have been set: "Direct Sun" for the FirstQube and SecondQube and "Umbral" for the optical ground station and its telescope. As a result, the accesses were calculated. For both of them, only 17 accesses were found over a month and with an average duration of 1 minute. Even if there are very few accesses, their average duration still makes them relevant for satellite tracking purposes. As far as satellite reflective detection, other important considerations should include the illumination angle of the satellite and the role of the seasons. However, these considerations are beyond the scope of this thesis, so they are left for detailed future analysis once the final mission concept is chosen.

On the other hand, for LED beacon detection the satellite should preferably not be sun-illuminated. Therefore, two more sunlight constraints have been set: "Umbral" for both the satellites and the optical ground station. No accesses have been found, meaning that the satellites are in sunlight 100% of the time in this particular time arc and with these orbital characteristics.

Chapter 5

GNSS Receiver High-Level Design

This chapter begins by providing the basics of GNSS, prior to perform a preliminary power analysis to estimate the power available for payload functioning. This analysis enables the identification of new GNSS payload system requirements, which will constraint the receiver research and selection. Eventually, a GNSS receiver will be tested through several hardware-in-the-loop (HIL) simulations with a GNSS signal simulator to verify its positioning measurements accuracy and power consumption.

5.1 The Basics of Global Navigation Satellite System

A satellite-based navigation system is a system that uses satellite constellations to provide Positioning, Navigation, and Timing (PNT) services. A constellation with global coverage is called Global Navigation Satellite System (GNSS), which provides signals for PNT purposes. These signals are electromagnetic waves, propagating at the speed of light and at given frequencies. They are transmitted from the satellites towards GNSS receivers, which should receive and process the signals to determine their location.

The GNSS signals allows for three basic types of measurements, derived from Pseudorange, Carrier phase, and Doppler observations, which are crucial for computing receiver's position and velocity. As defined in [44], the pseudorange measures the satellite-receiver distance measuring the difference between the receiver clock at signal reception and the satellite clock at signal transmission, scaled by the speed of light. However, these measurements are affected by receiver and satellite clock errors

and several other delays, which can be explained by the pseudorange observation equation [44]:

$$p_r^s = \rho_r^s + c(dt_r - dt^s) + T_r^s + I_r^s + e_r^s \quad (5.1)$$

where:

- ρ_r^s refers to the true geometric distance, calculated as the norm of the difference between the unknown position vector of the receiver and the unknown position vector of the satellite;
- c is the speed of light;
- dt_r and dt^s are the receiver and satellite clock errors, due to the asynchronicity between the two clocks;
- T_r^s is the electrically neutral atmosphere (troposphere and stratosphere) propagation delay;
- I_r^s is the ionosphere propagation delay, due to ionizing radiation impacting radio waves propagation;
- e_r^s includes other delay errors, such as the receiver noise.

A similar observation equation exists for carrier phase observation. These equations are valid considering a receiver placed on Earth, while they must be adjusted if the receiver is flying on a satellite in LEO, to account for several space factors, primarily the absence of atmospheric delays.

Typically, a receiver used for high-precision positioning applications provides users with raw data derived from pseudorange or carrier-phase observations to calculate the receiver's coordinates. In contrast, for more basic navigation applications, GNSS receivers offer an on-board navigation solution (NAVSOL), which is based on processed GNSS observation measurements, directly providing position, velocity, and time information.

As for position determination, the acquisition of latitude, longitude and altitude is referred to as "3-Dimensional Fix". To achieve it, a receiver must acquire signals from at least four GNSS satellites since, as explained in [44], their measurements are needed to estimate the three coordinates of the receiver and its clock error.

Currently, there are several global and regional navigation satellite systems in operation, such as: GPS (USA), GLONASS (Russia), Galileo (Europe), BeiDou (China), QZSS (Japan), IRNSS/NavIC (India).

5.2 Power Analysis

To determine suitable GNSS receivers for the mission, a power analysis was performed to identify how much power the EPS and, in particular, its solar arrays mounted on the satellites provide and, on the other hand, what the power consumption of the core bus subsystems is. In other words, a power budget was carried out to estimate the "surplus" power, a key information for not only for the GNSS selection, but also for the payloads final definition. Indeed, a low available power on-board could limit the spacecraft design and, as a consequence, also mission features.

The orbit average available power and the power consumption are usually calculated with reference to a certain operational phase, such as silent, detumbling¹, commissioning², nominal or safe modes. Continuing this high-level study, the power budget was performed only for nominal mode, which would require maximum average orbital power.

5.2.1 Orbit Average Available Power

In order to calculate the average power available in orbit, it is necessary to first specify the type of solar cells that will be mounted on the PocketQube, again a legacy of Delfi-PQ. These cells are 30% Triple Junction GaAs Solar Cell Assembly, type 3G30A, produced by Azurspace [47]. The solar cell characteristics of interest in this analysis were solar cell area, efficiency, and number of solar cells in Delfi-PQ, summarized in the following table.

¹"Detumbling refers to the act of dampening the angular velocity of the satellite." [45]

²"Commissioning is the first phase of satellite operations and begins immediately after deployment. It typically includes initial orbit determination and tracking [...]. [46]

Table 5.1 AzurSpace Solar Cell features and Number of Cells in a 3P PocketQube.

Area [cm^2]	Efficiency [%]	Number (3P PocketQube)
30.18	28.1	8

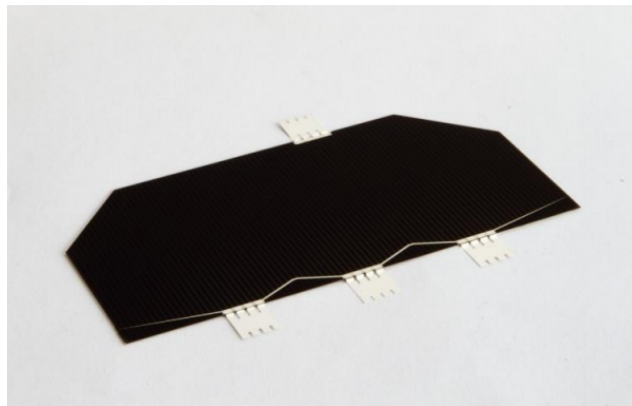


Fig. 5.1 AzurSpace Solar Cell, from its Datasheet.

The efficiency value shown is not the one reported in the datasheet [48], because it already takes into account the efficiency of both the solar cell and its coverglass, made by Qioptiq [49].

The orbit average available power was computed through STK. The model uploaded in STK was the one relative to the 3U CubeSat, as said in Chapter 3, thus the solar cells used are of two types, with the following characteristics.

Table 5.2 STK Solar Cell features and Number of Cells in the 3U CubeSat model.

	Area [cm^2]	Efficiency [%]	Number (3U CubeSat)
Large	26.56	28	24
Small	4	28	18

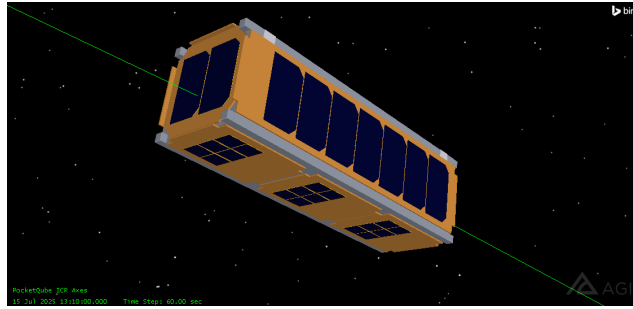


Fig. 5.2 Solar Cells of the 3U CubeSat model in STK.

Conversions were then implemented to run the power analysis directly with the CubeSat model in STK. These conversions were based on the simple equation:

$$(\text{Number of cells} * \text{Cell Area} * \text{Efficiency})_{3U} = (\text{Number of cells} * \text{Cell Area} * \text{Efficiency})_{3P}$$

Knowing the number of cells and area values, the efficiencies could have been easily calculated. They were $\eta_{large} = 9.122$ for large cells and $\eta_{small} = 1.308$ for small cells.

In addition, before launching the simulation, the attitude of the satellite was set. To account for random spinning, the satellite was set to rotate around two rotational axes, with an average rotation speed, equal to $\omega = 1.67 \text{ revs}/\text{min}$, based on Delfi-PQ available data.

Finally, the simulation was started using STK's Solar Panel Tool. From the generated report, the average power available in orbit was deduced.

$$P_{available} = 1.127 \text{ W}$$

5.2.2 Power Budget

The power budget is the allocation of power to each spacecraft element during the mission. It plays a crucial role in managing power demand to maintain a balance between power consumption and supply. In principle, the development of a power budget is also necessary to size the power generation, storage and distribution systems, which fulfill three of the main functions of the Electrical Power System. In this case, analysis of the space system avionic architecture and identification of the core bus subsystems power consumption will be helpful in quantifying the amount

of power available for payloads, in order to choose their number and typologies.

Table 5.3 TwinSat Mission Power Budget for Nominal Mode.

Subsystem	Mode	Maturity	BEE [mW]	BEE + Contingency [mW]	Duty Cycle	OAP [mW]
EPS	On	A	45.00	45.45	100.00%	45
CDH	On	A	30.00	30.30	100.00%	30
COMM	Receive	A	104.57	105.62	95.00%	100
	Transceive	A	371.62	375.34	8.30%	31
Total Consumed Power [mW]:						207
Total Available Power [mW]:						1127
Budget surplus / deficit [mW]:						920

The Table shows the mission power consumption breakdown, where:

- The **Best Engineering Estimate (BEE)** is the estimated resource value determined on the basis of past experiences, technical calculations or test, without considering the uncertainties associated to the design maturity [50]. The values shown in the Table derives from Delfi-PQ core-bus measurements.
- The **Contingency** is the resource differential, expressed usually as a percentage of the BEE, added to the BEE to cover the uncertainties due to the lack of design details [50]. The contingency varies according to the level of design maturity. In this study, the applied Contingency values are provided in the Table below.

Table 5.4 Contingency Values.

Maturity	Code	Contingency
Final Flight Hardware	A	1 %
Qualification Model	B	5 %
Engineering Model	C	10 %
Prototype Measurement	D	15 %
Circuit Estimate	E	25 %
Conceptual Estimate	F	30 %

- The **Duty Cycle** is the measure of the fraction or percentage of time a system is actively working within a given period of time. The value of duty cycles

depends on the operating mode. In this case, the nominal mode is expected to be the one with the maximum consumption, thus duty cycles are set at total percentage of 100%.

As can be noted from the Table 5.3, the total consumed power is equal to:

$$P_{consumed} = 0.207 \text{ W}$$

and, therefore, the amount of power available for payloads is:

$$P_{surplus} = P_{consumed} - P_{available} = 1.127 - 0.207 = 0.920 \text{ W}$$

5.2.3 Possible GNSS Receivers for the TU Delft Mission

The surplus amount of power is intended not only for the GNSS receiver, but also for some of the other payloads (see Subsection 1.2.4) that might be accommodated. Additionally, it has to be taken into account that the total power budget shall include a margin of at least 20% of the nominal power required for normal spacecraft operations [51]. Thus, starting from the surplus power value mentioned above, a requirement on the power allocated to the GNSS was set:

"The GNSS Receiver Power Consumption shall be less than 0.5 W."

In addition, another requirement was set on the size of the receiver. Considering that each board in a 3P PocketQube has a size of 42 mm x 42 mm and taking into account a margin from these dimensions, it was determined that:

"The GNSS Receiver Size shall be less than 40 mm x 30 mm."

By conducting a comprehensive research among space-capable and future candidates space-capable GNSS receivers, several devices suitable for this TU Delft mission were identified. It is worth clarifying that in this context the space-based designation can be established either if the receiver has a track record of use in past space missions or the manufacturer explicitly states that it is suitable for use in space [52].

The characteristics of the receivers are summarized in the following Table, adapted from [52].

Table 5.5 Space-capable and future candidate space-capable GNSS Receivers suitable for the TwinSat Mission. *N/A stands for Not Available.

Model Supplier	Space-Capable (SC) \\ Future Candidate (FC)	Power [W]	Mass [gr]	Size [mm]
Orion B16-C Navspark	SC	0.21	1.6	12 x 16 x 3
GPS module WARPSpace	SC	0.15	3	24 x 24 x 5
S1216F8-GI3 SkyTraq	FC	0.40	2	12 x 16
S1216F8-GL SkyTraq	FC	0.13	1.6	12.2 x 16
PX1122C SkyTraq	FC	0.17	1.7	12 x 16
Venus816 SkyTraq	FC	0.07	0.3 (estimate)	5 x 5
Venus828F SkyTraq	FC	0.07	0.2	7 x 7 x 1.4
Venus838FLPx SkyTraq	FC	0.1	0.3	10 x 10 x 1.3
TESEO-LIV3F STMicroelectronics N.V.	FC	0.08	N/A*	9.7 x 10
STA8089G STMicroelectronics N.V.	FC	0.04	N/A*	7 x 7 x 1.0
MAX-M8C u-blox	FC	0.07	2.0 (estimate)	9.7 x 10.1 x 2.5
MAX-M8Q u-blox	FC	0.07	2.0 (estimate)	9.7 x 10.1 x 2.5
MAX-M8W u-blox	FC	0.07	2.0 (estimate)	9.7 x 10.1 x 2.5
NEO-M8Q-01A u-blox	FC	0.07	2.0 (estimate)	12.2 x 16.0 x 2.4
ZED-F9P-04B u-blox	FC	0.07	2.0 (estimate)	17 x 22 x 2.4

Furthermore, a very promising receiver appears to be the QLX300+ GNSS receiver, currently under development by Qualinx. The company's goal is to provide a power-

efficient sensor [53], with ten times less power consumption than other devices currently available.

To choose a receiver, further trade-offs could be made based on particular Figures of Merit. However, it is known that the Delfi Team would prefer receivers that have not yet flown, for technology demonstration reasons. Also, the Team has already purchased two SkyTraq receivers, thus the analyses in the next chapters will focus on the following receivers:

- **SkyTraq PX1122C**: it is a dual-frequency (GPS L1/L2C) receiver. In addition to the features already mentioned, this device is a real-time kinematic (RTK) receiver designed to reach cm-level position accuracy for precision guidance application and relative positioning. Indeed, it can provide raw measurements to perform carrier phase RTK processing, as mentioned in its Datasheet ([54], referred to version -R).



Fig. 5.3 SkyTraq PX1122C GNSS Receiver.

- **SkyTraq S1216F8-GI3**: as for GPS, it receive only L1 frequency. This receiver, used for vehicle navigation, asset tracking and time synchronization applications [55], cannot provide raw measurements.



Fig. 5.4 SkyTraq S1216F8-GI3 GNSS Receiver.

COordinating COMmittee for Multilateral export controls³-free firmware can be applied to both receivers for use in space. Given its characteristics, the dual-frequency receiver may be the best option as a payload, but both receivers will still be tested.

5.3 GNSS Signal Emulation

The main objective of these new analyses is to test the accuracy of the GNSS receiver in returning the satellite position data and, at the same time, verify the power consumption of the receiver in use. To achieve these goals, a GNSS signal was emulated and transmitted to the receiver. Comparison of the input files, used to emulate the GNSS signal, and the output files, with the positions calculated by the receiver, allowed the accuracy of the receiver to be estimated.

5.3.1 Software-Defined GPS Signal Simulator (GPS-SDR-SIM)

The GPS signal simulation in this thesis was developed based on the open-source software, GPS-SDR-SIM [56]. Once the user specifies a static location or a trajectory (user motion file) and a GPS satellite constellation by providing a recorded GPS ephemeris files (RINEX navigation file), the GPS-SDR-SIM generates GPS baseband signal data streams, which include simulated pseudorange and Doppler information for the GPS satellites in view. These data streams can be converted to Radio-Frequency signals for offline testing through a Software-Defined Radio (SDR) platform.

The User Motion File (UMF) can be given in:

- **Static mode:** the input location is specified in Latitude Longitude Altitude (LLA) format;
- **Dynamic mode:** the user motion file can be specified in either ECEF, LLA or NMEA GGA⁴ format.

³The CoCom limit refers to a constraint placed on GNSS receivers that limits their functionality if the device is beyond a maximum altitude or moving faster than a specific speed.

⁴NMEA GGA stands for "Global Positioning System Fix Data" and it is a protocol header used in the NMEA 0183 standard.

It is also possible to specify a scenario start time, which can correspond to the first time of the ephemeris in the RINEX navigation file. When the binary file, called "gpssim.bin", has been created, it can be transmitted to the receiver for playback, as will be explained later.

5.3.2 GNSS Receiver Software

To visualize the data while monitoring the SkyTraq receivers in real-time, a NAVSpark GNSS Viewer software was used. This software displays the NMEA standard messages, which contain valuable information provided by the receiver after achieving the lock on GNSS signals. In this analyses, NMEA GGA messages will be extracted from the receiver, providing its time, position and fix type data.

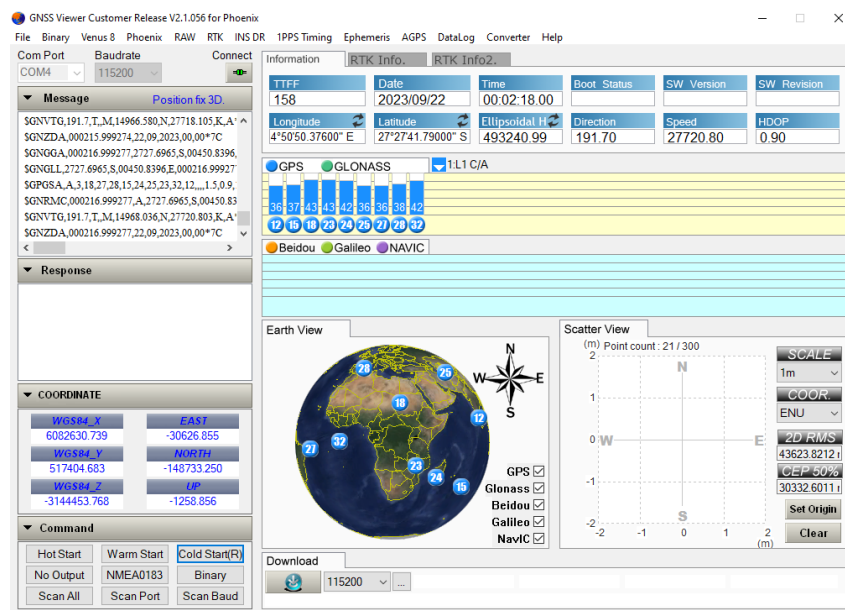


Fig. 5.5 Screenshot of the GNSS Viewer Software interface after the receiver has acquired the 3D-Fix during a simulation.

As can be seen from the interface shown above, in addition to the data extracted from NMEA messages, the viewer directly shows several parameters. Some of the most useful include:

- Positioning information: Date, Time, Latitude, Longitude, Ellipsoidal Height, Direction, Speed, HPOP (Horizontal Dilution of Precision);

- The number of satellite in view and the signal quality in terms of SNR (Signal-to-Noise Ratio);
- Time To First Fix (TTFF) and accuracy of position fix, shown in a scatter diagram and expressed as 2D RMS (Root Mean Square) or 50% CEP (Circular Error Probability).

Furthermore, the viewer allows us to send commands to the receiver to change the output of incoming messages (from NMEA to Binary, for instance), or to restart the receiver with Hot, Warm or Cold Start commands.

In the simulations that follow, this software was used to first verify the acquisition of the 3D Fix by reading the incoming data, before using other methods to extract the data.

5.3.3 Hardware-In-The-Loop Simulation: Setup and Process

The HIL simulation is a testing and validation technique that provides emulation environment capabilities that allow the integration of real equipment into the simulation [57]. A HIL simulation was performed to test the GNSS receiver in a simulated environment. Before showing the results, the simulation setup will be introduced and the process followed will be explained below.

Setup

The simulation was run on a computer owned by TU Delft, on which the GPS-SDR-SIM software is installed. The setup of the experiment consists of:

- A USRP B200 **software-defined radio** developed by Ettus [58]. The platform has a continuous frequency coverage from 70 MHz – 6 GHz.
- A **signal manual attenuator** used for electronic signal calibration and noise reduction. The Model 50DR-143, a 50 Ohm manual step attenuator with attenuation range 0 to 80dB by 1dB steps, was used [59].
- A **DC-Block** is a component used to block DC voltage while allowing RF signals to pass through with minimal loss. The model used is the BLK-18-S+ with 50 Ohm impedance [60].



Fig. 5.6 URSP Radio (a) and Attenuator (b).

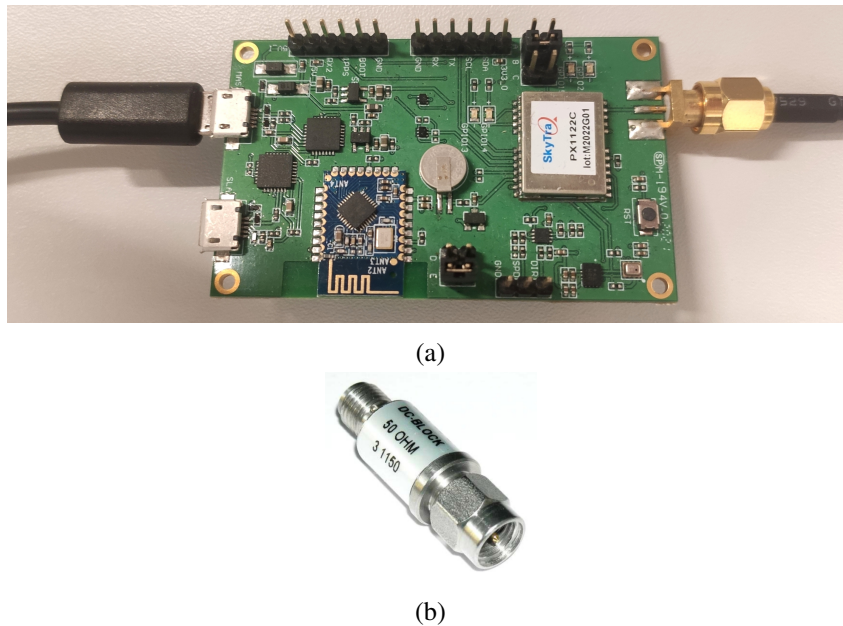


Fig. 5.7 SkyTraq PX1122C GNSS Receiver installed on its board (a) and DC Block (b).

During the simulations, the SDR platform transmitter port is connected to the board (right side of Figure 5.7a) of the GPS receiver under test through an attenuator, fixed at 30 dB, and a DC block. The receiver board is then connected to the computer

via a USB cable (left side of Figure 5.7a) in order to communicate with the GNSS receiver software and extract the calculated data.

Process

The process followed in these simulations was as follows:

1. Download the daily GPS broadcast ephemeris, the Rinex navigation file, from [61]. In this case, the author downloaded the "brdc2650.23n" updated to 22 September 2023.
2. Generate the binary file, specifying one of the following command lines on the GNU Radio⁵ Command Prompt:
 - For a static mode simulation:
gps-sdr-sim -e Rinex\brdc2650.23n -l Lat,Lon,Hei
where a static location is given by its LLA coordinates;
 - For a dynamic mode simulation:
gps-sdr-sim -e Rinex\brdc2650.23n -u usermotion.csv
where the user motion file is given in ECEF x,y,z format.

As said, the binary file will be automatically saved as "gpssim.bin". Moreover, in this command line, the simulation start time can be also specified, if the corresponding set of ephemerides is available. Alternatively, the first time of ephemeris in the RINEX navigation file is selected [56].

3. Create an empty log.csv file where to save the logged data.
4. Read the data from the GNSS receiver. For this purpose there are several methods, but in this case, a previous python file, named "serial_reader.py," was used and suitably modified to extract the desired data. Run the following command line on Anaconda Command Prompt, referring to the file created in the previous step:

• **python serial_reader_mc.py -l log.csv**

⁵GNU Radio is a free and open-source software development toolkit that provides signal processing blocks to implement software radios. [62]

The script requires setting the correct communication port and entering the baud rate⁶, set at 115200. A crucial modification to this script enabled to force a cold start of the receiver each time the script is launched. As a consequence, the time required for 3D acquisition turns out to be the cold start TTFF.

5. Playback the binary file. Run the following command line on GNU Radio Command Prompt:

- `python gps-sdr-sim-uhd.py -t gpssim.bin -s 2600000 -x 30`

where "gps-sdr-sim-uhd.py" is a Python file present in the GPS-SDR-SIM software suite, "2600000" is the sampling rate to be used and "30" is the RF gain to be used.

6. Wait for the 3D Fix to be acquired and then lost, at the end of the log.csv file playback. The duration of playback depends strictly on the length of the user motion file.
7. Stop the programs and check the filled log.csv file.

5.3.4 Hardware-In-The-Loop Simulation: Accuracy of the GNSS Receiver

The first simulation, static, was performed with SkyTraq PX1122C, giving as input the LLA coordinates of the radio ground station inserted in the STK scenario:

Table 5.6 Latitude, Longitude and Altitude coordinates of the radio ground station given as input for the simulation with SkyTraq PX1122C receiver.

Radio Ground Station	
Latitude	51.998 °
Longitude	4.3734°
Altitude	90 m

The acquisition of the 3D fix was then verified. However, the author's primary focus is on dynamic simulations. Inserting a trajectory into the user motion file and

⁶The baud rate is a measure of the data transmission rate and define the number of signal or symbol changes that occur per second in a data transmission.

simulating a GPS signal as it would be received by a receiver in space enables realistic testing of the receiver performance. This approach provides insights into the receiver accuracy when acquiring a 3D fix under real-world conditions. Unfortunately, updating the GNSS receiver firmware to make it CoCom-free was not possible. As a result, the maximum operational altitude of the dual-frequency receiver remains limited to 80 km.

For this reason, it was decided to launch the dynamic simulations directly with the SkyTraq S1216F8-GI3 receiver, on which CoCom-free firmware could be installed instead.

The first point to be addressed is the definition of the user motion file to provide as input. Due to a system limitation, only user motion of maximum duration 300 time instants (divided between 0.0 and 300.0 in 0.1 second steps) can be given to the GPS-SDR-SIM software. Accordingly, 4 trajectory arcs of 5-minute duration were extracted from STK. In particular, they were extracted from the Sequence-2 scenario, which includes both relative distance and relative velocity stopping conditions (see Subsection 3.1.3 and Figure 4.8). These trajectory arcs were named as follows:

1. **Initial State**, which refers to the first 5-minute arc of the scenario;
2. **Increase**, related to an arc around the first conjunction between the two satellites;
3. **Conjunction**, that is an arc relative to the time when one of the two satellites doubles its drag area;
4. **Stop Scenario**, that refers to an arc taken on the last day of the scenario.

The coordinates downloaded from STK are Cartesian coordinates taken with respect to the ECI reference system. Through a MATLAB script, they were transformed into ECEF coordinates, which is the correct format to be supplied to the GPS-SDR-SIM software. As a result, four user motion files were created, each consisting of four columns: the first is for relative time and the other three are the ECEF coordinates. Here is an example:

Table 5.7 User Motion File for "Initial State" trajectory arc.

Relative Time	x_{ECEF}^{UMF} [m]	y_{ECEF}^{UMF} [m]	z_{ECEF}^{UMF} [m]
0	-2716906	-6318773	17113.3
0.1	-2717043	-6318712	17868.04
0.2	-2717180	-6318651	18622.79
0.3	-2717316	-6318590	19377.53
0.4	-2717453	-6318529	20132.28
...
299.6	-2962298	-5790235	2236021
299.7	-2962322	-5789947	2236734
299.8	-2962346	-5789659	2237447
299.9	-2962370	-5789371	2238160
300	-2962394	-5789083	2238872

These user motion files, along with the Rinex navigation file, were used to create the binary files. The start time of the scenario was also set equal to the start instant of the RINEX file. In fact, as is already known, the trajectories of the STK scenario are relative to 2025, but the GPS-SDR-SIM software would not support a future date, whose ephemeris are not available. Therefore, since the main interest is to understand whether this receiver is able to achieve a 3D fix and produce data independently of a precise date, the starting point given as input coincides with the first instant of the RINEX file, i.e., 22/09/2023 at 00:00:00 UTC. Following the steps explained in the previous section, the binary files were then transmitted to the GNSS receiver, and logs file with position data were obtained from it. All four simulations successfully acquired the 3D fix. An example of log file, for the "Initial State" trajectory arc, is shown below:

Table 5.8 Log File for "Initial State" trajectory arc.

UTC Time	UTC Date	Latitude	Longitude	Altitude	Fix Type
11:59:45	28/06/2006	0.0 N	0.0 E	0.0 m	No
11:59:46	28/06/2006	0.0 N	0.0 E	0.0 m	No
11:59:47	28/06/2006	0.0 N	0.0 E	0.0 m	No
...
12:00:37	28/06/2006	0.0 N	0.0 E	0.0 m	No
12:00:38	28/06/2006	0.0 N	0.0 E	0.0 m	No
12:00:39	28/06/2006	0.0 N	0.0 E	0.0 m	No
00:00:19	22/09/2023	0.0 N	0.0 E	0.0 m	No
00:00:20	22/09/2023	0.0 N	0.0 E	0.0 m	No
00:00:21	22/09/2023	0.0 N	0.0 E	0.0 m	No
...
00:00:24	22/09/2023	0.0 N	0.0 E	0.0 m	No
00:00:25	22/09/2023	2.844 N	113.798 W	500092.0 m	3D
00:00:26	22/09/2023	2.908 N	113.811 W	500100.8 m	3D
00:00:27	22/09/2023	2.971 N	113.823 W	500093.6 m	3D
00:00:28	22/09/2023	3.034 N	113.836 W	500088.5 m	3D
00:00:29	22/09/2023	3.098 N	113.848 W	500101.1 m	3D
00:00:30	22/09/2023	3.161 N	113.861 W	500093.0 m	3D
...
00:04:43	22/09/2023	19.108 N	117.099 W	501830.1 m	3D
00:04:44	22/09/2023	19.108 N	117.099 W	501830.1 m	3D
00:04:45	22/09/2023	19.108 N	117.099 W	501830.1 m	3D
00:04:46	22/09/2023	19.108 N	117.099 W	501830.1 m	No
00:04:47	22/09/2023	19.108 N	117.099 W	501830.1 m	No
00:04:48	22/09/2023	19.108 N	117.099 W	501830.1 m	No

As can be seen, the file starts at 11:59:45 UTC on 28/06/2006, the time at which the cold start of the receiver occurs. Then, the receiver first acquires the actual time and date, relative to the signal the radio is transmitting and, after a few seconds, also acquires the 3D fix. The time elapsed between the cold start and the acquisition of the lock is the cold start TTFF, which will be useful in the power consumption analysis discussed in the next subsection.

The GNSS 3D Fix provides position data in LLA coordinates, with latitude and

longitude measured in degrees with directional indicators⁷ in reference to the Earth's equator and prime meridian. Altitude is measured in meters above the WGS84 reference ellipsoid. Therefore, in order to compare the log files, obtained as output from the receiver, with the user motion files, which contain the initial trajectories, it is necessary to:

- Transform the LLA coordinates of the log files into ECEF coordinates;
- Correlate the UTC time of the log.csv to the relative time of the usermotion.csv file.

These two points were addressed in another MATLAB script, which appropriately modifies the log files so that they can be cross-referenced with the user motion files. The script also deals with post-processing of the data. Having the Cartesian coordinates of the ECEF available in the three directions, a 3-dimensional graph was first derived:

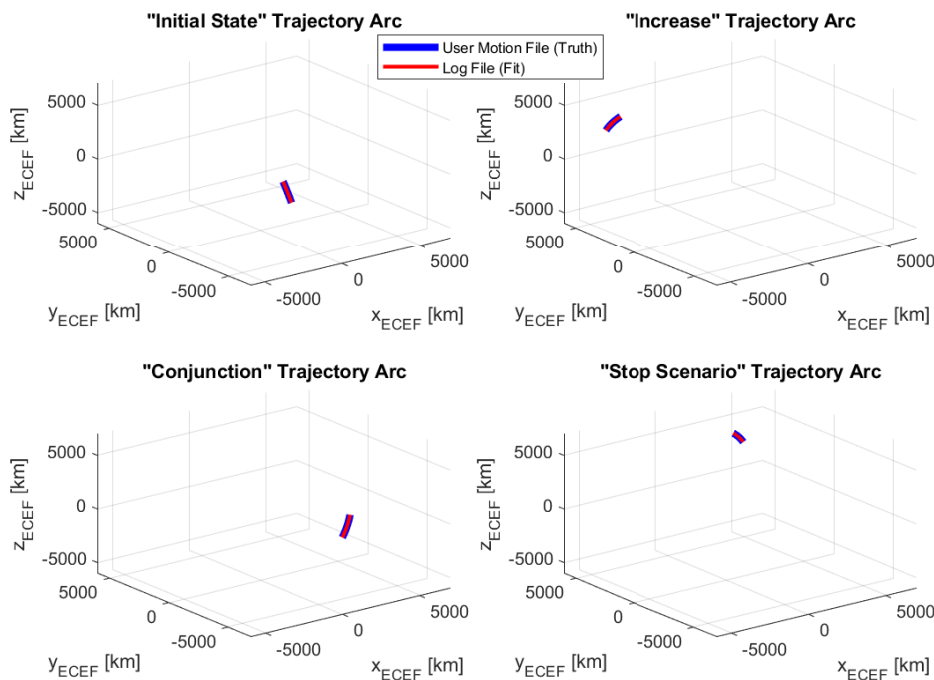


Fig. 5.8 The 3D graphs show the nearly perfect overlap between the input position (in blue) and the simulated position (in red). The axis limits are specified.

⁷They are: North (N), South (S), East (E), West (W).

On a kilometer scale, it appears that the log trajectory arc (fit) overlaps perfectly with the user motion one (truth). To more accurately show the position error, it is estimated as the difference of the input position and the simulated position, along each of the three directions. These differences are computed as follows:

$$\begin{aligned}\Delta x &= x_{ECEF}^{UMF} - x_{ECEF}^{LOG} \\ \Delta y &= y_{ECEF}^{UMF} - y_{ECEF}^{LOG} \\ \Delta z &= z_{ECEF}^{UMF} - z_{ECEF}^{LOG}\end{aligned}\quad (5.2)$$

The graphs showing the differences in the four different cases are reported:

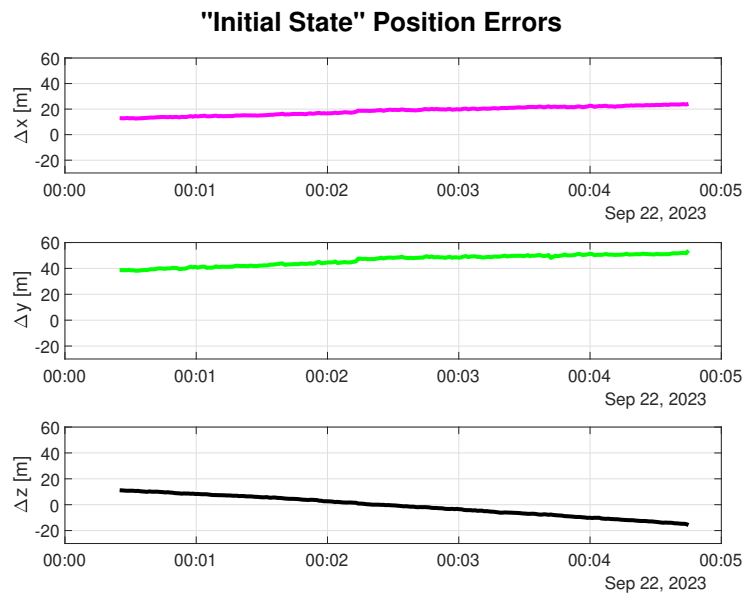


Fig. 5.9 Position Errors related to "Initial State" Trajectory Arc.

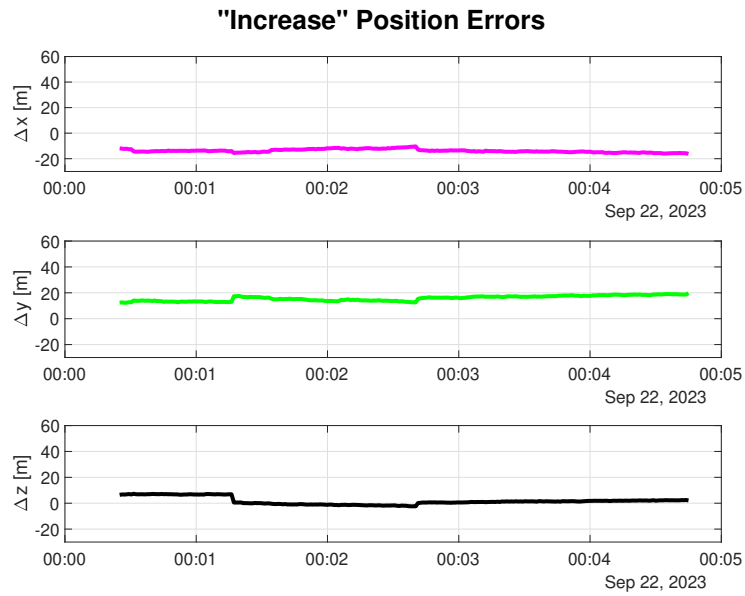


Fig. 5.10 Position Errors related to "Increase" Trajectory Arc.

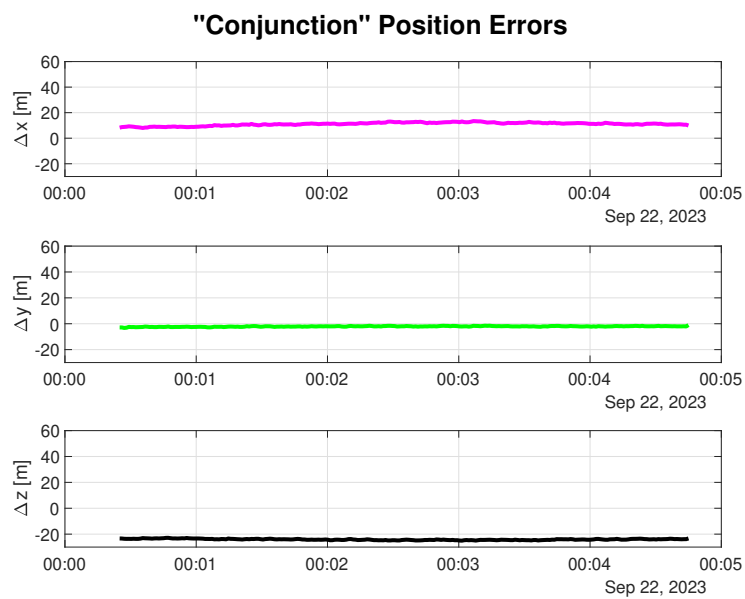


Fig. 5.11 Position Errors related to "Conjunction" Trajectory Arc.

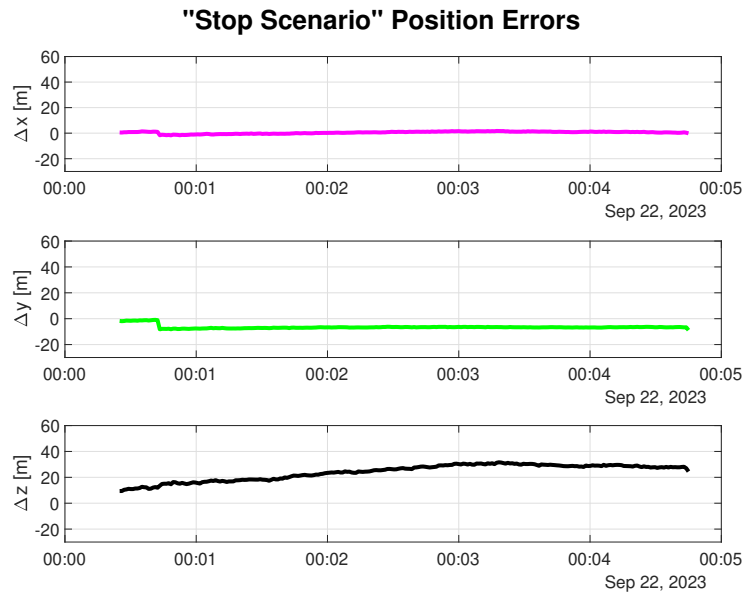


Fig. 5.12 Position Errors related to "Stop Scenario" Trajectory Arc.

As can be seen from the graphs, the error is on the order of units or tens of meters in each different direction. To get a clearer overall view of the error, the Root Mean Square Error (RMSE) was calculated, using the following formula:

$$rmse = \sqrt{\Delta x^2 + \Delta y^2 + \Delta z^2} \quad (5.3)$$

For each of the four trajectory arcs under consideration, the RMSE turned out to be:

$$\begin{aligned} rmse_1 &= 50.8 \text{ m} \\ rmse_2 &= 21.4 \text{ m} \\ rmse_3 &= 26.6 \text{ m} \\ rmse_4 &= 25.7 \text{ m} \end{aligned} \quad (5.4)$$

As stated in the Datasheet [55], the accuracy of this receiver should be about 2.5 m CEP accuracy. The accuracy found is higher, ranging between 20 m and 50 m RMS error. However, these measurements are reliable for the following reasons:

- The accuracy of the software that generates the binary files, simulating GNSS signals, is unknown. The software does not compensate for ionospheric refraction, leading to an error;
- In contrast, the receiver used in this HIL simulations applied ionospheric correction, resulting in an additional error of a few meters. For a single-frequency GNSS receiver, the ionospheric refraction is one of the main error sources, which particularly impacts the altitude component of a position solution for a ground-based receiver or the radial component if the receiver is flying on-board a LEO satellite [63]. Moreover, the ionospheric refraction at LEO altitude can vary a lot with respect to a GNSS receiver placed at the ground. In this case, to optimize performances, the option of the receiver to correct for the ionospheric refraction should be disabled;
- For COTS receivers such as the one under consideration, NAVSOL also involve a periodic error to be attributed to the receiver real-time navigation algorithm. In fact, it does not account for Coriolis acceleration, an apparent force that, however, becomes non-negligible at the high velocities at which the satellite moves, as stated in [63]. To verify this error, one should extract and post-process NAVSOL in terms of radial, along-track and out-of-plane components. Indeed, the effect of Coriolis acceleration should result in a periodic bias in the out-of-plane component for both NAVSOL positions and velocities. However, the paper referred to was published only few weeks ago, when most of this work was already performed, therefore this error should be properly investigated and verified in the future with further research.

In addition, the first error of 50.8 m, which is rather high compared to the others, could be explained by the fact that "Initial State" is the only trajectory arc in which the satellite is crossing the equatorial region, with a latitude of 0° . In fact, as demonstrated in [63], by fitting the orbital models to NAVSOL (positions and velocities), it is possible to identify several errors in the estimation of orbital parameters, thus in orbit determination. Most notably, in their research, they state that the RAAN estimate is affected by an error due to a systematic rotation of the orbital plane, which then causes a periodic error with maximum magnitude at the equator, where it is on the order of tens of meters.

5.3.5 GNSS Receiver Power Consumption

The power consumption of the SkyTraq S1216F8-GI3 receiver was obtained by connecting the receiver to a power supply during data transmission. It was found to be 110 mA at 3.3 V, in accordance with what is written in its Datasheet [55].

To calculate the total consumption of the GNSS receiver payload when operational, the other components of the board that will accommodate it inside the satellite must also be considered: these are an low-noise amplifier (LNA), with consumption of 10 mA at 3.3 V, and a processor/SD card, with consumption of 15 mA at 3.3 V.

Combining the three main players, the total consumption of the GNSS receiver payload in nominal mode turned out to be:

$$P_{GNSS} = 0.135 \text{ W}$$

which is in accordance with the requirement initially established (see Appendix A). As a consequence, the mission power budget was updated as follows:

Table 5.9 Updated TwinSat Mission Power Budget for Nominal Mode, taking into account GNSS receiver payload power consumption.

Subsystem	Mode	Maturity	BEE [mW]	BEE + Contingency [mW]	Duty Cycle	OAP [mW]
EPS	On	A	45.00	45.45	100.00%	45
CDH	On	A	30.00	30.30	100.00%	30
COMM	Receive	A	104.57	105.62	95.00%	100
	Transceive	A	371.62	375.34	8.30%	31
GNSS receiver	On	F	135.00	175.50	100.00%	176
Total Consumed Power [mW]:						383
Total Available Power [mW]:						1127
Budget surplus / deficit [mW]:						744

Hence, around 0.74 W of power are still available to accommodate the other payloads.

Chapter 6

Conclusions and Future Work

In this last chapter, the main results derived from this research work will be discussed and, finally, some possible ideas for future work will be outlined.

6.1 Conclusions

Over the course of this thesis, the high-level mission analysis and system design of a picosatellites cluster were performed, within the context of a new TU Delft small satellite mission for technology demonstration and SSA improvement purposes. The mission primary goals are to demonstrate in-space and ground precise tracking of multiple formation-flying pico- of femto-satellites.

Once chosen Extreme A to investigate, the mission space segment included two identical and independent 3P PocketQubes. Launched as a single spacecraft, the satellites will be separated in orbit by a spring force release and fly in formation. Throughout Chapter 3 and 4, several mission scenarios were explored by defining two MCSs in STK: Sequence 1, with satellite propagation stopping conditions based only on relative distance, and Sequence 2, with stopping conditions based on relative distance and relative velocity. Both the sequences were also characterized by updates in spacecraft properties, such as variations in the drag area of the satellites, to model their relative motion by means of differential-drag. The execution of the MCSs in different steps, acting on the two satellites in the same simulation, and the iteration of different parameters were possible because of the interface between STK and MATLAB.

Taking into account a satellite separation in the In-Track direction, some initial simulations results showed that initial relative velocity shall be equal to 10 cm/s, value in accordance with a literature review, while a drag area increment factor of 2x shall be provided to guarantee satellites to orbit in close proximity for an adequate amount of time.

Considering the aforementioned requirements and comparing the two MCSs, Sequence 2 was found to be the most effective: after their separation, satellites move away less fast, so they can orbit in a specified spatial range longer than with Sequence 1 (their conjunctions occur later in time) and, most importantly, there is a significant reduction in the time the satellites spend in with increased drag. Therefore, implementing a scenario with Sequence 2 the satellites would loss less altitude in the same time frame and their lifetime would be extended. On the other hand, in this scenario there is no control over the minimum distance that satellites would reach during their conjunctions, thus further research would be needed.

To complete the picture, given the separation velocity requirement, other separation directions in which it is safe to separate satellites were checked, to account for the possible presence of a satellite spin that would not ensure separation along the In-Track direction. A region of space resembling a cone with a vertex at the satellite's center of mass and a half-aperture angle of 52.7 degrees was defined: with a separation within this region, the satellite relative distance at their first close passage, after one orbit, is greater than 1 km, which is the safety limit value established for collision avoidance.

Through DRAMA simulations, the mission duration was also estimated: due to a smaller average cross-sectional area, the scenario with Sequence 2 provided a duration of 7.5 months, which is 1.5 months longer than the 6 months guaranteed by Sequence 1, reflecting the initial requirement on the months required for in-orbit testing.

Eventually, the contact time between the satellite and the ground segment was investigated, including all necessary constraints. With respect to the mission analysis period under consideration, an adequate amount of accesses was ensured with both a radio and optical ground station.

After outlining and describing this possible mission concept, further analysis was performed in Chapter 5 to estimate the power available for payload operations. Through STK Solar Panel Tool, the orbit average available power was estimated and found to be around 1.1 W. This information allowed the Power Budget, calculated

for nominal mode, to close with a power surplus of about 0.9 W available to allocate payloads.

Among them, it was chosen to analyze the GNSS receiver as it provides another way to calculate satellites position and velocity in real time.

As a consequence of the power analysis, a requirement was established on the required power for the GNSS receiver, set at 0.5 W, followed by another requirement on this payload size (< 40 mm x 30 mm).

Space-capable COTS receivers suitable for this mission and currently available on the market were identified, focusing on two SkyTraq receivers: PX1122C, which is dual-frequency and can provide raw measurements, and S1216F8-GI3, which is single-frequency and cannot provide raw data.

To test the accuracy of these receivers in returning satellite's position and to verify their power consumption in nominal mode, multiple GNSS signal emulation analyses were performed through the GPS-SDR-SIM software. However, it was discovered that the dual-frequency receiver firmware had a CoCom limit which restricted the maximum operational altitude to 80 km, and could not be updated. Therefore, dynamic simulations were carried out only with the single-frequency receiver: they consisted of comparing an input user motion file, with a 300-second trajectory arc entered to simulate a GPS signal as it would be received by a receiver on-board a LEO satellite, and the output file, which includes the positions calculated by the receiver.

Four different trajectory arcs were extracted from STK Sequence-2 scenario and gave as input to the GPS-SDR-SIM software. All four simulations successfully acquired the 3D Fix and four log files, with position data, were recorded.

By post-processing the data, it was possible to compare user motion and log files, showing that the RMS error is equal to 50 m for the first trajectory arc and between 20 m and 30 m for the others. Although quite high, these values are reliable because of several software and receiver limits that must be taken into account, and should be overcome with further research, in order to achieve GNSS receiver accuracy of a few meters.

6.2 Future Work

The mission and system requirements obtained can be used as the basis for further mission analysis and for future iterations of payload design, thus they will be subject to an iterative process as the TU Delft mission project progresses. Moreover, during the development of the thesis, several suggestions for additional research emerged, both to enhance already explored topics and to present new concepts that may be of remarkable interest in the future.

With respect to the mission analysis, the most interesting points for future work are:

- **Extreme B Mission Concept study.** Further mission analysis should investigate Extreme B mission concept, which includes a 3U CubeSat which will deploy a cluster of smaller satellites, to highlight its possible advantages and drawbacks compared to the Extreme A mission concept studied in detail in this thesis;
- **Extension of the duration of analysis.** In this thesis, the focus was on the first months (1-4) of the scenario. The analysis period should increase to study long-term effects;
- **Satellite control strategy optimization to minimize collision risk.** It was seen that the Sequence-2 scenario has many advantages over the Sequence-1 scenario. However, as mentioned above, in this scenario there is no control over the minimum distance during conjunctions, which reaches peaks of 100 meters. These values are far below the limit considered critical for collision risk (set at 1 km) and, therefore, it would be necessary to act on the drag area variation even when the satellites are approaching, perhaps by placing a new stopping condition. The consequences of new variations in the drag area are to be explored. In this respect, it would be necessary to study a strategy for controlling the satellites that maximizes their safety;
- **Study of mechanisms.** The separation mechanism should be designed to ensure a specific separation velocity. The mechanism to increase the drag area, such as the use of an actuated solar panel, should also be investigated;

- **ADCS Design.** Inclusion of this system would guarantee a way to stabilize the attitude of the satellite, a key factor in drag area variations and power generation considerations.

With respect to the GNSS receiver preliminary design, the most interesting points for future work are:

- **Updating SkyTraq PX1122C GNSS Receiver firmware.** By updating its firmware, dynamic simulations can also be performed with this dual-frequency simulator, which is what the Delfi Team would prefer to use because of its ability to provide raw data;
- **Running simulations with longer trajectory arcs.** Current trajectory arcs are limited to 300 s due to user motion file limitations. The possibility of increasing the arc duration would allow the accuracy of the positioning measurements to be verified over a longer period, thus being able to see the magnitude of performance changes.
- **Overcoming the limits of the system to minimize the RMS error.** Further simulations have to be carried out to verify the sources of error in positioning measurements. Finally, one should improve the accuracy of the GPS signal simulator and improve some features (ionospheric correction, dynamic model applied in the real-time navigation algorithm) of the receiver by adapting them for use on-board a satellite flying in LEO.

References

- [1] Spremo S.M., Crocker A.R., and Panontin T.L. Small Spacecraft Overview. *NASA Small Spacecraft Systems Virtual Institute*, 2019.
- [2] ECSS Secretariat ESA-ESTEC. ECSS-E-ST-10-12C, Space engineering - methods for the calculation of radiation received and its effects, and a policy for design margins, 2008.
- [3] NASA Small Spacecraft Systems Virtual Institute. State-of-the-Art Small Spacecraft Technology, 2021.
- [4] NASA Small Spacecraft Systems Virtual Institute. State-of-the-Art Small Spacecraft Technology, 2023.
- [5] Kulu E. "PocketQubes". [Online] Accessed: Aug 4, 2023.
- [6] Twigg B. Making it Small. *Cal Poly Developers' Workshop, California State Polytechnic University*, 2009.
- [7] Gunter D. Krebs. "Falcon-9 v1.2 (Block 5) (Falcon-9FT (Block 5))". *Gunter's Space Page*. [Online] Accessed: Aug 4, 2023.
- [8] Alba Orbital, TU Delft, and Gauss Srl. The PocketQube Standard. Issue 1, 2018. [Online] Accessed: Aug 4, 2023. Available at: <https://www.albaorbital.com/pocketqube-standard>.
- [9] TU Delft. Delfi Program. [Online] Accessed: Aug 23, 2023. Available at: <https://www.tudelft.nl/lr/delfi-space/delfi-program>.
- [10] Radu S., Uludag M.S., Speretta S., Bouwmeester J., Gill E., and Chronas Foteinakis N. Delfi-PQ: The first pocketqube of Delft University of Technology. *Proceedings of 69th International Astronautical Congress: Bremen, Germany*, [IAC-18-B4.6B. 5] International Astronautical Federation, IAF., 2018.
- [11] ECSS Secretariat ESA-ESTEC. ECSS-M-ST-10C Rev. 1, Space project management - Project planning and implementation, 2012.
- [12] Grego L. Update of UCS Satellite Database. [Online] Accessed: Aug 27, 2023. Available at: <https://blog.ucsusa.org/lgrego/update-of-ucs-satellite-database-2/>.

- [13] Union of Concerned Scientists. UCS Satellite Database. [Online] Accessed: Aug 27, 2023. Available at: <https://www.ucsusa.org/resources/satellite-database>.
- [14] Executive Office of the President. National Space Traffic Management Policy - Space Policy Directive-3. *Federal Register*, 83:28969–28976, 2018.
- [15] European Union Agency for Space Programme. Space Situational Awareness. [Online] Accessed: Aug 27, 2023. Available at: <https://www.euspa.europa.eu/european-space/space-situational-awareness>.
- [16] Speretta S., Uludag M.S., Menicucci A., and Ferrario I. Space Surveillance Network Capabilities Evaluation Mission. *Proceedings of 2nd NEO and Debris Detection Conference*, 2, 2023.
- [17] United States Government Accountability Office. Large Constellations of Satellites. Mitigating Environmental and Other Effects, 2022.
- [18] Seitzer P. et al. Optical Tracking and Attitude Determination of LEO CubeSats with LEDs: A Balloon Demonstration. *AMOS Technologies Conference, Maui, Hawaii*, 2018.
- [19] Marzioli P. et al. Usage of Light Emitting Diodes (LEDs) for improved satellite tracking. *Acta Astronautica*, 179:228–237, 2023.
- [20] Scott Balch M., Martin R., and Ferson S. Satellite conjunction analysis and the false confidence theorem. *Proc. R. Soc. A*, 475:20180565, 2019.
- [21] ESA TEC - Directorate of Technology, Engineering and Quality. Space Debris Mitigation. [Online] Accessed: Sep 18, 2023. Available at: <https://ecss.nl/>.
- [22] Voss H.D., Dailey J.F., Orvis M.B, White A.J., and Brandle S. From Globalstar Link: From Reentry Altitude and Beyond. *Proceedings of 30th Annual AIAA/USU Conference on Small Satellites*, 2016.
- [23] Curtis H. *Orbital Mechanics for Engineering Students*. Elsevier, 2005.
- [24] Bate R.R., Mueller D.D., White J.E., and Saylor W.W. *Fundamentals of Astrodynamics - Second Edition*. Dover, 2021.
- [25] Ansys Inc. "Technical Notes for HPOP". [Online] Accessed: Oct 6, 2023. Available at: <https://help.ansi.com/stk/>.
- [26] Tapley B.D., Shutz B.E., and Born G.H. *Statistical Orbit Determination*. Elsevier, 2004.
- [27] Kumar B.S., Ng A., Yoshihara K., and De Ruiter A. Differential Drag as a Means of Spacecraft Formation Control. *IEEE Transactions on Aerospace and Electronic Systems*, 2011.

- [28] Ansys Inc. "HPOP Force Models > Drag". [Online] Accessed: Oct 6, 2023. Available at: <https://help.ansi.com/stk/>.
- [29] NASA. *Rendezvous and Proximity Operations Handbook Part 2*. Mission Operations Directorate, 1988.
- [30] Ansys Inc. "Ansys STK". [Online] Accessed: Aug 5, 2023. Available at: <https://www.ansi.com/products/missions/ansi-stk>.
- [31] Ansys Inc. "Astrogator". [Online] Accessed: Aug 5, 2023. Available at: <https://help.ansi.com/stk/>.
- [32] Ansys Inc. "Set Scenario Properties". [Online] Accessed: Aug 6, 2023. Available at: <https://help.ansi.com/stk/>.
- [33] ECSS Secretariat ESA-ESTEC. ECSS-S-ST-00-01C, ECSS system - Glossary of Terms, 2009.
- [34] Bouwmeester J. et al. Utility and constraints of PocketQubes. *CEAS Space Journal*, 12:573–586, 2020.
- [35] Ansys Inc. "Stopping Conditions". [Online] Accessed: Aug 7, 2023. Available at: <https://help.ansi.com/stk/>.
- [36] Ansys Inc. "STK Programming Interface". [Online] Accessed: Sep 3, 2023. Available at: <https://help.ansi.com/stkdevkit/11.0/>.
- [37] Ansys Inc. "MATLAB: Connect via COM". [Online] Accessed: Sep 3, 2023. Available at: <https://help.ansi.com/stk/>.
- [38] ESA ESOC. "Space Debris User Portal". [Online] Accessed: Sep 20, 2023. Available at: <https://sdup.esoc.esa.int/>.
- [39] Hiler R. Design of a CubeSat Separation Mechanism. *Honors Theses*, 2794, 2017.
- [40] Burton R., Laystrom-Woodard J., Benavides G., Carroll D., Coverston V., Swenson G., Pukniel A., Chosh A., and Moctezuma A. Initial development of the cubesail/ultrasail spacecraft. *Joint Army Navy NASA Air Force (JANNAF) Spacecraft Propulsion Subcommittee Meeting*, 2010.
- [41] Luo Y.Z., Sun Z.J., and Zhang J. Proximity scenario design for geostationary rendezvous with collocated satellite avoidance. *Acta Astronautica*, 154:153–168, 2019.
- [42] MathWorks. "movmean". [Online] Accessed: Sep 3, 2023. Available at: <https://it.mathworks.com/help/matlab/ref/movmean.html>.
- [43] Hobbs S., Stansbery G., and Matos de Carvalho T. *Waste (Second Edition) - Chapter 30 - Space Waste*. Elsevier, 2019.

- [44] Teunissen P.J.G. and Montenbruck O. *Handbook of Global Navigation Satellite Systems*. Springer, 2017.
- [45] Yadav J. and Goyal T. Investigation of Instabilities in Detumbling Algorithms. *IEEE Aerospace Conference*, 2020.
- [46] SSRI Knowledge Space Resources for smallsat success. Operations > Commissioning. [Online] Accessed: Oct 9, 2023. Available at: <https://s3vi.ndc.nasa.gov/ssri-kb/>.
- [47] Azur Space. Home. [Online] Accessed: Oct 9, 2023. Available at: <https://www.azurspace.com/index.php/en/>.
- [48] Azur Space. TJ Solar Cell Assembly 3G30A - Datasheet. [Online] Accessed: Oct 9, 2023. Available at: <https://www.azurspace.com/index.php/en/products/products-space/space-assemblies>.
- [49] Qioptiq. Solar Cell Coverglasses. [Online] Accessed: Oct 9, 2023. Available at: <https://www.excelitas.com/product/space-qualified-cover-glass>.
- [50] Corpino S. Slide of "Space Mission and System Design" Course. *Politecnico di Torino*, 2021.
- [51] ESA ESTEC. Margin philosophy for science assessment studies. *European Space Agency*, 2012.
- [52] Gill E., Morton J., Axelrad P., Akos D.M., Centrella M., and Speretta S. Overview of Space-Capable Global Navigation Satellite Systems Receivers: Heritage, Status and the Trend towards Miniaturization. *Sensors*, 2023, 23, 7648.
- [53] Qualinx. Trusted Universal Tracking and Connectivity Solution. [Online] Accessed: Oct 10, 2023. Available at: <https://qualinx.io/>.
- [54] SkyTraq Technology Inc. "PX1122R". [Online] Accessed: Oct 10, 2023. Available at: <https://www.skytraq.com.tw/homesite/home-product>.
- [55] SkyTraq Technology Inc. "S1216F8-GI3". [Online] Accessed: Oct 10, 2023. Available at: <https://www.skytraq.com.tw/homesite/home-product>.
- [56] Ebinuma T. "GPS-SDR-SIM". [Online] Accessed: Oct 10, 2023. Available at: <https://github.com/osqzss/gps-sdr-sim>.
- [57] Edgar T.W. and Manz D.O. *Research Methods for Cyber Security - Chapter 8 - Using Simulation for Research*. Elsevier, 2017.
- [58] Digilent Company. "Ettus USRP B200: 1x1, 70MHz-6GHz SDR/Cognitive Radio". [Online] Accessed: Oct 10, 2023. Available at: <https://diligent.com/shop/ettus-usrp-b200-1x1-70mhz-6ghz-sdr-cognitive-radio/>.

-
- [59] JFW Industries. "Manual Attenuator DC-3000MHz 0-80dB x 1dB | 50DR-143". [Online] Accessed: Oct 10, 2023. Available at: <https://www.jfwindustries.com/product/50dr-143-dual-rotary-attenuator/>.
- [60] American Radio Supply. "50-Ohm DC Block 0.01 to 18 GHz SMA". [Online] Accessed: Oct 10, 2023. Available at: <https://www.americanradiosupply.com/50-ohm-dc-block-0-01-to-18-ghz-sma-ars-4556/>.
- [61] NASA. "Earth Data - Crustal Dynamics Data Information System". [Online] Accessed: Oct 10, 2023. Available at: <https://cddis.nasa.gov/archive/gnss/data/daily/>.
- [62] Gnu Radio. "GNURadio - The free and open software radio ecosystem". [Online] Accessed: Oct 10, 2023. Available at: <https://github.com/gnuradio/gnuradio>.
- [63] Müller L., Chen K., Möller G., Rothacher M., Soja B., and Lopez L. Real-time navigation solutions of low-cost off-the-shelf GNSS receivers on board the Astrocass constellation satellites. *Advances in Space Research*, 2023.
- [64] NASA. NASA Systems Engineering Handbook, 2007.
- [65] ECSS Secretariat ESA-ESTEC. ECSS-E-ST-10-02C, Space engineering - Verification, 2009.
- [66] ECSS Secretariat ESA-ESTEC. ECSS-E-ST-10-06C, Space engineering - Technical requirements specification, 2009.

Appendix A

Technical Requirement Specification

Requirements elicitation is a process that starts from the stakeholders expectations to develop a set of mission, system, subsystem and component technical requirements. As stated in the NASA System Engineering Handbook [64], the requirements, expressed as "shall" statements, must first be validated with respect to stakeholder needs, the mission goals and constraints, the concept of operations, and the mission success criteria. For this purpose, it should be checked if the technical requirements are written correctly, technically correct, feasible, verifiable, redundant, over-specified and if they satisfy stakeholders.

In particular, each requirement should be unique and therefore it is characterised by an alphanumeric identifier (ID). In this work, the IDs are directly correlated to several Configuration Items¹ (CIs), which are shown in Table A.1.

As the requirements are developed, their verification method should be defined. Approved verification methods include [65]:

- **Test (T)** (including demonstration). Verification by test shall consist of measuring product performance and functions under representative simulated environments.
- **Analysis (A)** (including similarity). Verification by analysis shall consist of performing theoretical or empirical evaluation using techniques agreed with the Customer.

¹Configuration Items are defined as "Any hardware, software, or combination of both that satisfies an end use function and is designated for separate configuration management. [64]"

Table A.1 Configuration Items.

Identifier (ID)	Configuration Item
MIS	Mission
SAT	Satellite Space Segment
CDH	Command and Data Handling System
COMM	Communication System
EPS	Electrical Power System
STR	Structural System
MEC	Mechanisms System
TCS	Thermal Control System
PAY	Payloads
GRS	Ground Segment
PGR	Payload Ground Segment

- **Review-Of-Design (ROD).** Verification by Review-of design shall consist of using approved records or evidence that unambiguously show that the requirement is met.
- **Inspection (I).** Verification by inspection shall consist of visual determination of physical characteristics.

Eventually, the requirements have also been classified through different categories as outlined in the Technical Requirements Specification ECSS guidelines. Among them, the types of requirements that will be mentioned are [66]:

- **Functional Requirements** are requirements that define what the product shall perform, in order to conform to the needs / mission statement or requirements of the user.
- **Mission Requirements** are requirements related to a task, a function, a constraint, or an action induced by the mission scenario.
- **Environmental Requirements** are requirements related to a product or the system environment during its life cycle; this includes the natural environments and induced environments.
- **Physical Requirements** are requirements that establish the boundary conditions to ensure physical compatibility and that are not defined by the interface requirements, design and construction requirements, or referenced drawings.

- **Design Requirements** are requirements related to the imposed design and construction standards such as design standards, selection list of components or materials, interchangeability, safety or margins.

A.1 Initial Mission and System Requirements

The starting technical requirements are listed in Table A.3.

A.2 New Mission and System Requirements

The requirements derived as a result of the high-level mission analysis are shown in Table A.4.

A.3 Applicable and Reference Documents

The Applicable Documents ([21], Chapter 5, Chapter 4) are documents which are directly mentioned in a "shall" statement, while the Reference Documents are documents which are referenced in this Technical Requirement Specification and that provide additional information throughout the requirement definition process.

Table A.2 Applicable and Reference Documents.

Applicable Documents	
AD01	ESA Space Debris Mitigation Guidelines
AD02	Chapter 5: GNSS Receiver High-Level Design
AD03	Chapter 4: Simulation Results and High-Level Requirements
Reference Documents	
RD01	ECSS-E-ST-10-06C Space Engineering - Technical Requirements Specification
RD02	ECSS-E-ST-10-02C Space Engineering - Verification
RD03	NASA Systems Engineering Handbook

Table A.3 Initial Mission and Systems Requirements.

Configuration Item	Category	ID	Requirement	Verification Method
Mission	Mission	MIS-010	Two 3P PocketQubes shall at least be developed.	RoD, I
Mission	Mission	MIS-020	The mission shall target a launch in 2025.	RoD
Mission	Mission	MIS-030	The critical mission lifetime shall be equal to at least 6 months.	RoD, A
Mission	Mission	MIS-040	The satellites shall be released in an orbital range of 475-525 km.	RoD
Mission	Mission	MIS-050	The separation of the satellites shall occur upon command.	RoD
Mission	Mission	MIS-060	The characteristics for the lowest orbit possible shall be limited by a minimum mission lifetime equal to the critical mission lifetime.	RoD, A
Mission	Mission	MIS-070	The orbit inclination range shall be 95-105 deg.	RoD
Mission	Mission	MIS-080	The mission cost shall be less than 300k Euro, including launch and operations.	RoD
Mission	Design	MIS-090	The mission shall be compliant with ESA's Space Debris Mitigation Guidelines [AD01].	RoD
Satellite Space Segment	Functional	SAT-010	Each satellite must be equipped with a core segment with space heritage.	RoD
Satellite Space Segment	Functional	SAT-020	The core segment of each satellite shall be composed of the following subsystems*: EPS, CDH, COMM, STR, TCS.	RoD
Satellite Space Segment	Physical	SAT-030	The space segment mass shall be less than 1.5 kg.	I
Satellite Space Segment	Environmental	SAT-040	All systems of the each satellite shall survive the launch environment.	A, T
Satellite Space Segment	Environmental	SAT-050	All systems of each satellite shall be able to cope with the space environment.	RoD
Satellite Space Segment	Mission	SAT-060	All systems of each satellite shall be compliant with the power budget as described in [AD02].	RoD, T
Payload	Functional	PAY-010	Each satellite shall provide independent position measurements.	RoD
Payload	Mission	PAY-020	Each satellite shall be equipped with a Global Navigation Satellite System (GNSS) Receiver.	RoD
Payload Ground Segment	Functional	PGR-010	The optical ground station should be able to track the satellites.	A
Payload Ground Segment	Functional	PGR-020	The optical ground station shall meet an elevation constraint of at least 45 degrees.	RoD
Payload Ground Segment	Functional	PRS-030	The laser ground station should be able to track the satellites.	A
Ground Segment	Functional	GRS-010	The radar ground station should be able to track the satellites.	A
Ground Segment	Functional	GRS-020	The radio ground station should be able to track the satellites.	A
Ground Segment	Functional	GRS-030	The radio ground station shall meet an elevation constraint of at least 5 degrees.	RoD

* EPS = Electrical Power System; CHD = Command and Data Handling System; COMM = Communication System; STR = Structural System; TCS = Thermal Control System.

Table A.4 New Mission and Systems Requirements.

Configuration Item	Category	ID	Requirement	Verification Method
Mission	Mission	MIS-100	The initial relative Separation Velocity shall be equal to 10 cm/s.	RoD, A
Mission	Mission	MIS-110	The Drag Area shall be increased and decreased by a factor of two.	RoD, A
Mission	Mission	MIS-120	The Drag Area variations shall be managed by a control strategy that takes into account at least relative distance and relative velocity.	RoD, A
Mission	Mission	MIS-130	The satellite separation shall occur within the region of space bounded by a cone (Fig. 4.22 of [AD03]) centered in one of the satellites center of mass and with a maximum half-aperture angle of 52.7°.	RoD, A
Payload	Functional	PAY-030	The GNSS Receiver Power Consumption shall be less than 0.5 W.	RoD, I
Payload	Physical	PAY-040	The GNSS Receiver Size shall be less than 40 mm x 30 mm.	RoD, I